NASA TECHNICAL NOTE

NASA TN D-3444

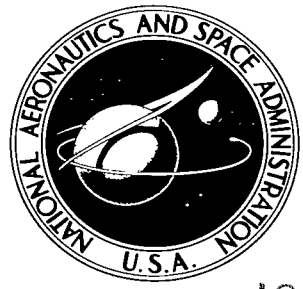

NASA TN D-3444

AN EXPERIMENTAL STUDY OF THE OXIDATION OF GRAPHITE IN HIGH-TEMPERATURE SUPERSONIC AND HYPERSONIC ENVIRONMENTS

by Irvin M. Miller and Kenneth Sutton

Langley Research Center
Langley Station, Hampton, Va.

NATIONAL AERONAUTICS AND SPACE ADMINISTRATION • WASHINGTON, D. C. • JULY 1966

AN EXPERIMENTAL STUDY OF THE OXIDATION OF GRAPHITE IN HIGH-TEMPERATURE SUPERSONIC AND HYPERSONIC ENVIRONMENTS

By Irvin M. Miller and Kenneth Sutton

Langley Research Center
Langley Station, Hampton, Va.

NATIONAL AERONAUTICS AND SPACE ADMINISTRATION

For sale by the Clearinghouse for Federal Scientific and Technical Information
Springfield, Virginia 22151 – Price $2.00

AN EXPERIMENTAL STUDY OF THE OXIDATION OF GRAPHITE IN HIGH-TEMPERATURE SUPERSONIC AND HYPERSONIC ENVIRONMENTS

By Irvin M. Miller and Kenneth Sutton
Langley Research Center

SUMMARY

An experimental study was made of the oxidation of graphite exposed to high-temperature supersonic and hypersonic test streams of air and air-nitrogen mixtures. Oxidation-rate data were obtained on hemispherical-shaped models of three grades of graphite over wide ranges of aerothermal parameters to define the oxidation behavior of graphite and to compare this behavior with diffusion-controlled theory.

Models of ATJ graphite maintained a smooth shape and oxidized in a consistent manner at a rate below the maximum theoretical rate for diffusion-controlled reactions over a wide range of test conditions. However, most of the models of AHDG and AGSX graphite became distorted at oxygen-mass-flux levels above 0.03 lbm/ft^2-sec (0.146 kg/m^2-s) and at stagnation pressures behind the shock wave above 5.17 atmospheres. Because of equipment limitations, the stagnation pressure and oxygen-mass-flux levels at which this phenomenon begins was not determined. Furthermore, the distorted models of these two grades lost mass in an unpredictable and catastrophic manner at rates ranging up to $2\frac{1}{2}$ times the maximum rate for diffusion-controlled theory. At present, the factors which could explain the distortion effect in AHDG and AGSX graphites are not known.

INTRODUCTION

Graphite is being considered for use in hyperthermal environments because of its superior strength-weight ratio at temperatures above 3500° R (1940° K), relatively low cost, high thermal conductivity, high resistance to thermal shock, high emissivity, and ease in machining. A serious disadvantage to the use of graphite is that it begins to oxidize to a gaseous product at temperatures below 1000° R (560° K) with a consequent loss of material. In order to predict the performance of graphite for various flight missions, it is necessary to have an understanding of its oxidation behavior over a wide range of aerothermal parameters (such as pressure and oxygen concentration). Furthermore, an understanding of this oxidation behavior may result in an improved comprehension of

the oxidation behavior of carbonaceous chars which are formed on charring ablators, a class of materials being considered for reentry heat-shield applications.

The reaction of graphite with oxygen in a flowing airstream is either chemically controlled, diffusion controlled, or a combination of these, depending on the surface temperature. (See ref. 1.) A chemically controlled reaction occurs at lower surface temperatures where an excess of oxygen is present at the graphite surface, and the reaction rate depends only on the chemical kinetics of graphite and oxygen. At higher surface temperatures the oxygen supply at the surface becomes rapidly depleted, and the reaction rate becomes limited by the rate at which oxygen diffuses to the reacting surface. The rate of this diffusion-controlled reaction is therefore a function of the oxygen mass flux to the surface.

Numerous papers have been published on the chemically controlled oxidation of carbon and graphite in static or low-flow-rate oxidizing environments. (For example, see refs. 2 and 3.) The results of such studies, which are usually given in some form of the Arrhenius equation, have shown a wide variation in reaction rates which is generally thought to be due to differences in the materials tested. Some theoretical papers have shown that the diffusion-controlled oxidation of graphite should be influenced by the aerodynamic characteristics of the airstream and body shape (see ref. 3); however, data on the oxidation behavior of graphite have not been adequate to allow a prediction of this behavior over a range of environmental conditions. One experimental study conducted in a hypersonic environment (ref. 4) yielded a limited amount of data for defining the effect of aerothermal parameters on oxidation rates.

Most aerothermal structural applications being considered for graphite and charring ablators involve high surface temperatures between 2800° R (1560° K) and 5000° R (2780° K) at which diffusion-controlled reactions are expected. (See ref. 5.) Therefore, the primary purpose of the present experimental study was to investigate the oxidation behavior of graphite at surface temperatures above 2800° R (1560° K) as a function of aerothermal parameters in high-temperature supersonic and hypersonic environments and to compare this behavior with existing theory.

The experimental program was carried out with three grades of graphite to determine whether a variation in physical properties would affect oxidation behavior. Wide ranges of aerothermal parameters were included in the program by exposing hemispherical graphite models with diameters between 0.375 and 1 inch (0.953 and 2.54 cm) to the jets of three test facilities: the Langley 11-inch ceramic-heated tunnel, the arc-heated materials jet at the Langley Research Center, and the Langley 20-inch hypersonic arc-heated tunnel. The oxygen content in the jets of the latter two facilities was varied to increase the range of oxygen mass flux. The stagnation pressure behind the shock wave was varied from 0.06 to 8.28 atmospheres, the stagnation enthalpy was varied from

595 to 4080 Btu/lbm (1.38 to 9.47 MJ/kg), and the oxygen mass fraction was varied from 0.059 to 0.232.

SYMBOLS

The units used for the physical quantities defined in this paper are given both in the U.S. Customary Units and in the International System of Units (SI). (See ref. 6.) Appendix A is included for the purpose of explaining the relationships between these two systems of units.

c	mass fraction of oxygen
H	enthalpy, Btu/lbm (MJ/kg)
k	specific reaction rate, $lbm/ft^2\text{-}sec\text{-}atm^{\alpha}$ $\left(kg/m^2\text{-}s\text{-}(N/m^2)^{\alpha}\right)$
M	Mach number
$\dot{m}$	mass-transfer rate, $lbm/ft^2\text{-}sec$ $(kg/m^2\text{-}s)$
N_{Pr}	Prandtl number
p	pressure, atm (1 atm = 101325 N/m^2)
q	heat-transfer rate, $Btu/ft^2\text{-}sec$ (MW/m^2)
r	model radius, in. (cm)
T	temperature, ^{o}R (^{o}K)
t	time, sec (s)
x	mole fraction of oxygen
α	order of the reaction
β	blowing coefficient
λ	mass of carbon reacted per unit mass of oxygen consumed

Subscripts:

C	carbon
e	at the outer edge of the thermal or concentration boundary layer

O	oxygen
t,2	stagnation condition behind the shock wave
w	at the wall

METHODS AND TESTS

Models and Techniques

The hemispherical-shaped models used in the present study were machined to 0.375-inch (0.953-cm), 0.5-inch (1.27-cm), and 1-inch (2.54-cm) diameters, as shown by the drawing in figure 1. This range in model size was included to aid in varying the heat-transfer rate to the stagnation point. Three grades of graphite were used: AHDG, AGSX, and ATJ. These grades were selected to determine whether different graphite grades would have different oxidation rates under diffusion-controlled conditions. Some properties of the different graphite grades, as given by each manufacturer, are summarized in table I.

Test conditions were chosen to obtain a wide variation in the important aerothermal parameters expected to influence the oxidation of graphite. These parameters were stagnation pressure, stagnation enthalpy, and stream mass fraction of oxygen. Stagnation pressure in the present report always refers to the stagnation pressure behind the shock wave. In order to obtain a wide variation of test conditions, models were tested in three different facilities at the Langley Research Center: the Langley 11-inch ceramic-heated tunnel, the arc-heated materials jet at the Langley Research Center, and the Langley 20-inch hypersonic arc-heated tunnel. Test conditions used in the study are shown for each facility in table II.

The Langley 11-inch ceramic-heated tunnel, described in reference 7, was adapted with a Mach 2 nozzle having an exit diameter of 1.332 inches (3.38 cm). This arrangement provided airstreams in which the model size and/or stagnation pressure were varied (see table II) to obtain a range of oxygen mass flux at high stagnation-pressure levels. This range of oxygen mass flux at high stagnation-pressure levels was extended by the use of the arc-heated materials jet, described in reference 8, which was equipped with a Mach 2 nozzle having a 0.738-inch (1.874-cm) exit diameter and an air-nitrogen mixing system. A broad range of oxygen mass flux was obtained by varying the volume ratio of air to nitrogen in the test stream. The Langley 20-inch hypersonic arc-heated tunnel described in reference 9 and shown in figure 2 was used to provide air and air-nitrogen test streams in which the stagnation pressure and air-nitrogen volume ratio were varied at low stagnation-pressure levels to extend further the range of oxygen mass flux. A Mach 6 nozzle with an exit diameter of 6.6 inches (16.76 cm) was used in this tunnel.

The test streams for all these facilities had low contamination levels. The arc-heated jet and arc-heated tunnel utilize water-cooled copper electrodes and, as reported in reference 8, produce airstreams with less than 0.1 percent contamination. The ceramic-heated tunnel had a low-mass-flow airstream with a large ceramic pebble bed, and tests of graphite models in a cold airstream from this system indicated no significant erosion of graphite models due to dust contamination.

The models were held in the test stream by water-cooled stings. Models, model holders, and sting assemblies are shown in figure 3 for the 0.375-inch-diameter (0.953-cm) and 1-inch-diameter (2.54-cm) models. The assembly for the 0.5-inch-diameter (1.27-cm) model is similar in appearance to that for the 0.375-inch-diameter (0.953-cm) model. The four-model holder shown in figure 3(c) was used only in the hypersonic arc-heated facility where four 0.375-inch-diameter (0.953-cm) models could be tested simultaneously because of the large size of the nozzle exit.

In all three facilities the test procedure was generally the same. The test facility and instrumentation were programed for a specific run time. After flow stabilization was obtained in the test stream of the facility, movie cameras and a photographic pyrometer were turned on, and the model was inserted into the center of the test stream. The model was removed from the test stream at the specific test time or earlier if it appeared to oxidize rapidly. Movie cameras and a photographic pyrometer were used to record the recession of the model, and the photographic pyrometer was used to record model surface temperatures. In many of the runs an optical pyrometer was also used to measure the surface temperature at the stagnation point and to aid in observing the model under test. For most of the runs made in the supersonic arc-heated materials jet only the optical pyrometer was used to measure surface temperature.

Instrumentation and Data Reduction

The surface temperature of the model at the stagnation point was measured in most of the runs by a photographic pyrometer described in reference 10. This instrument was chosen because it provided a permanent measurement record of the model surface temperature at and near the stagnation point with a measurement error under the conditions of the test of about ± 4 percent. Data were recorded every second for shorter runs and every other second for longer runs. The optical pyrometer, used either with the photographic pyrometer or alone, was calibrated with a standard lamp source and was found to have an error of less than ± 2 percent. Measured surface temperatures were corrected for emissivity with a value of 0.77. (See ref. 11.)

Model recession and shape change were recorded by 16-mm black and white and color film in cameras operated at 64 or 400 frames per second and also by 35-mm film in the photographic pyrometer operated at 20 frames per second. Data reduction of the

receded model length on the 16-mm film was accomplished with the aid of a movie projector equipped with a still frame device and a frame counter. The projected length of the image was measured by a linear scale within an accuracy of about 1.5 percent. The elapsed time was determined, within an accuracy of a fraction of a second, by dividing the number of elapsed frames by the predetermined framing rate. Data reduction of the receded model length on the 35-mm film was accomplished with the aid of a contour projector equipped with a mechanical stage and micrometer dials. The projected length of this image was measured with an error of about 1.5 percent.

In order to determine the recession rate of the model, the model length was plotted as a function of time, and a straight line was drawn through the data representing a linear decrease of model length with time. This rate was converted to mass loss rate by multiplication by the nominal density of the graphite. The accuracy of the nominal density of the graphite was checked by measuring the density of about three models of each graphite grade and was found to be within ±4 percent of the measured density. Mass loss rates were considered to be accurate within ±5 percent.

Oxygen mass flux, the parameter influencing diffusion-controlled reactions, was not measured; it was computed from a known value, the stream mass fraction of oxygen, and a computed value, the heat-transfer coefficient. Values of oxygen mass flux so computed are valid at the stagnation point of smooth surfaces and are based on the initial shape of the model; hence, they are listed as reference oxygen mass flux on the figures to be presented. The equations used to compute oxygen mass flux are discussed in appendix B.

Since the purpose of the present study was to define the oxidation behavior of graphite at surface temperatures above 2800° R (1560° K) where diffusion-controlled reactions are expected, the data for surface temperatures below 2800° R (1560° K) were excluded from the analysis and results.

RESULTS AND DISCUSSION

A marked difference in oxidation behavior was observed between ATJ graphite and the other two graphite grades tested (AHDG and AGSX). Models of ATJ graphite maintained a round shape and surface integrity over wide ranges of stagnation pressure and oxygen mass flux for extended time periods, as shown in figures 4 and 5. This type of behavior was observed for AHDG and AGSX graphite models at low stagnation pressures from 0.0606 to 0.197 atm, as shown in figures 6(a) and 7(a). At stagnation pressures above 5.17 atm and an oxygen mass flux exceeding 0.03 lbm/ft^2-sec (0.146 kg/m^2-s), however, many of the models became grossly distorted and revealed a highly irregular surface. An example of this phenomenon can be seen in figures 6(b) and 7(b). The

movies showed that the AHDG and AGSX graphite models became initially distorted in the area surrounding the stagnation region. If the models were kept in the test stream for longer periods of time, the distorted area expanded to consume the stagnation region. Models 3 and 4 of figure 6(b) are AHDG graphite models which were removed with the stagnation region intact, whereas model 5 is an AHDG graphite model which became completely distorted. Most of the AGSX graphite models became completely distorted, as shown by models 4 and 5 in figure 7(b). The distorted model shapes observed for 0.5-inch-diameter (1.27-cm) models of AHDG and AGSX graphite were also observed for 1-inch-diameter (2.54-cm) models of the same grades, an indication that the distortion effect is not influenced by model size. (See figs. 8 and 9.) Tables III, IV, and V show the test parameters and observed results for all models.

In addition to the marked difference found in model shape behavior between ATJ graphite and the other two graphite grades tested, a difference was also found in the mass loss rate, as shown in figures 10, 11, and 12. These three figures show the oxidation rate plotted as a function of oxygen mass flux, which is considered to be the primary variable controlling diffusion-controlled reactions. (See ref. 1.) For comparison, all three figures show a theoretical carbon monoxide (CO) curve (the upper limit for diffusion-controlled reactions) and a theoretical carbon dioxide (CO_2) curve (the lower limit for diffusion-controlled reactions). The latter curve is based on the assumption that CO_2 is the predominant effective product for diffusion-controlled reactions (see ref. 12). These curves are defined by equations and supporting references in appendix B.

Figure 10 shows that the oxidation-rate data for ATJ graphite in all test environments followed a linear relationship with oxygen mass flux and fell between the theoretical CO and CO_2 curves. The data obtained in the arc-heated jet and the ceramic-heated tunnel indicated agreement over the range of oxygen mass flux common to both facilities.

Figures 11 and 12 show that at low levels of stagnation pressure and oxygen mass flux AHDG and AGSX graphite models maintained a smooth shape and oxidation rates were below the theoretical CO curve. However, at stagnation pressures above 5.17 atm and oxygen mass flux exceeding 0.03 lbm/ft^2-sec (0.146 kg/m^2-s), many of the graphite models became grossly distorted in shape, as previously noted, and mass loss rates for these models were highly erratic and unpredictable, ranging up to $2\frac{1}{2}$ times the theoretical maximum rate. Many of the models were removed from the stream with the stagnation region intact, and the oxidation rates for these models followed a pattern similar to the oxidation rates for ATJ graphite. This result suggests that if other graphite grades are tested under the same environmental conditions without becoming distorted, their oxidation rates would be similar to those for ATJ graphite. However, oxidation rates cannot presently be predicted for AHDG and AGSX graphite grades for stagnation pressures greater than 5.17 atm and for oxygen mass flux greater than 0.03 lbm/ft^2-sec

(0.146 kg/m^2-s). Because of the limitations of the test facilities, no data were available for stagnation pressures between 0.2 and 5.17 atm. Thus, the stagnation pressure at which model distortion and erratic oxidation rates become significant for AHDG and AGSX graphite grades was not determined.

Figures 10, 11, and 12 show a scattering of the oxidation-rate data for those models which did not become grossly distorted, and some of this scattering is believed to be due to variations in surface temperature. The importance of surface temperature is shown in figure 13, in which normalized rate data for the three grades of graphite tested are plotted as a function of this parameter. The normalized oxidation rate, a ratio of the experimental rate to the diffusion-limited rate for a CO product, was used to compare all data on the same basis. The plotted data show a surface-temperature effect between 2800° R (1560° K) and 3400° R (1890° K). When the data of figure 13 were separated into low- and high-stagnation-pressure ranges, as shown in figures 14 and 15, the surface-temperature effect was pronounced at low stagnation pressures up to 3800° R (2110° K) but was indeterminant at high stagnation pressures probably because of the narrow temperature range for most of the data. The results indicate that the scattering of the data in figures 10, 11, and 12 for those models which did not become grossly distorted is largely due to variations in surface temperature at low stagnation pressures, but is not understood at high stagnation pressures.

In order to help determine the oxidation mechanism at low stagnation pressures, pseudo activation energies were computed from the data at these low pressures. Values of pseudo activation energy from 10 to 13 kcal/g-mole (41.8 to 54.4 MJ/kg-mole) were found for the three grades of graphite for temperatures between 2800° R (1560° K) and 3800° R (2110° K). These values are intermediate between that found for diffusion-controlled reactions (4 kcal/g-mole (16.7 MJ/kg-mole); see ref. 2) and those found for chemically controlled reactions (17 to 44 kcal/g-mole (71 to 184 MJ/kg-mole); see ref. 3). These results indicate that for the range of surface temperatures between 2800° R (1560° K) and 3800° R (2110° K), oxidation may be occurring in a transition region between chemically controlled and diffusion-controlled reactions.

An analysis of oxidation data for surface temperatures between 3600° R (2000° K) and 3800° R (2110° K) suggested that the oxidation mechanism at this temperature level was nearly diffusion limited. This analysis was based on the theoretical prediction that if graphite is oxidized in air or air-nitrogen mixtures, the oxidation rate will depend upon both oxygen mass fraction and stagnation pressure in a unique manner, depending upon the oxidation mechanism. In a chemically controlled reaction, the oxidation rate depends on both variables raised to the same power; in a diffusion-controlled reaction, the oxidation rate depends on oxygen mass fraction raised to the first power and on stagnation pressure raised to the one-half power. (See appendix C.) If the theory is correct, log-log plots of

oxidation rate as a function of each variable would yield linear curves, the slope of each curve representing the power of the variable. Figures 16 and 17 show, for all three graphite grades, that the power of the oxygen mass fraction is about 1 and the power of the stagnation pressure is about 0.4.

Although the mechanism for initiating and maintaining the observed unpredictable and catastrophic oxidation behavior of AHDG and AGSX graphite is not known, it is of interest to point out the general conditions which appear to influence this behavior. Since the surface of the ATJ graphite models did not become rough and that of the AHDG and AGSX models did, the initiation of a rough surface appears to depend on the differences between graphite grades. These differences can be divided into three classes: (1) Chemical composition, such as impurities that may act as inhibitors or accelerators influencing the oxidation reaction; (2) physical properties, such as maximum grain size; and (3) processing technique, such as an extrusion or molding process. Many basic properties are included in these three classes, and the relation of these properties to oxidation behavior should be investigated in order to gain a better understanding of recession rate mechanisms.

Once the graphite surface has been initially roughened, the diffusion-controlled theory does not apply because the theory assumes a laminar boundary layer, and a roughened surface can be expected to produce turbulence with consequent higher rates of heat and mass transfer. One form of turbulence which can cause an accelerated transfer of oxygen to the surface is a horseshoe-shaped vortex which has been found to occur in the pits and cavities of a roughened surface. (See ref. 13.) Many of the tested models showed surface irregularities which appeared similar to those reported in this reference.

CONCLUSIONS

As a result of an experimental study of the oxidation behavior of graphite in high-temperature supersonic and hypersonic environments, the following conclusions are drawn:

1. Models of AHDG and AGSX graphite became grossly distorted in many cases at oxygen-mass-flux levels above 0.03 lbm/ft^2-sec (0.146 kg/m^2-s) and at stagnation pressures behind the shock wave above 5.17 atmospheres, whereas models of ATJ graphite maintained a smooth shape over a wide range of test conditions. Because of equipment limitations, the stagnation pressure and oxygen-mass-flux levels at which this phenomenon begins were not determined.

2. The oxidation rates of models of ATJ graphite followed a linear relation with oxygen mass flux between the theoretical CO and CO_2 curves over a wide range of oxygen flux, indicating that the oxidation of ATJ graphite is predictable for a wide range of

environments. The models of AHDG and AGSX graphite which became grossly distorted lost mass in an unpredictable manner at rates ranging up to $2\frac{1}{2}$ times the theoretical maximum rate.

3. The mechanism responsible for the distortion of AHDG and AGSX graphite and the mass loss rate behavior of these two graphites are not presently understood.

4. The oxidation-rate data for the models of AHDG and AGSX graphite with the stagnation region intact followed a pattern similar to that for ATJ graphite; these results indicate that if other graphite grades are tested under the same environmental conditions without becoming distorted their oxidation rates would be similar to those for ATJ graphite.

5. Since the factors accounting for the difference in oxidation behavior between the graphite grades studied are not known, the behavior of other graphite grades or carbonaceous chars in like environments cannot be predicted until such factors are determined.

6. The normalized oxidation rates for all three grades of graphite tested appeared to be temperature dependent at low stagnation pressures (0.06 to 0.20 atm) for surface temperatures between 2800° R (1560° K) and 3400° R (1890° K). This temperature range may represent a transition region between chemically controlled and diffusion-controlled reactions.

7. An anlysis of the data for surface temperatures above 3600° R (2000° K) showed evidence of a diffusion-controlled reaction for all three grades of graphite.

Langley Research Center,
National Aeronautics and Space Administration,
Langley Station, Hampton, Va., January 19, 1966.

APPENDIX A

CONVERSION OF U.S. CUSTOMARY UNITS TO SI UNITS

The International System of Units (SI) was adopted in 1960 by the Eleventh General Conference on Weights and Measures held in Paris, France. Conversion factors required for units used herein are given in the following table:

Physical quantity	U.S. Customary Unit	Conversion factor (*)	SI Unit
Activation energy	kcal/g-mole	4.18	MJ/kg-mole
Density	g/cm^3	1000	kg/m^3
Enthalpy	Btu/lbm	2.32×10^{-3}	MJ/kg
Heat-transfer rate	Btu/ft^2-sec	0.01135	MW/m^2
Length	in.	2.54	cm
Mass-transfer rate	lbm/ft^2-sec	4.88	kg/m^2-s
Mass-transfer rate × square root of nose radius	$lbm/ft^{3/2}$-sec	2.70	$kg/m^{3/2}$-s
Pressure	atm	1.01325×10^5	N/m^2
Temperature	^oR	5/9	^oK

*Multiply value given in U.S. Customary Unit by conversion factor to obtain equivalent value in SI unit.

Prefixes to indicate multiples of units are:

Prefix	Multiple
mega (M)	10^6
centi (c)	10^{-2}
milli (m)	10^{-3}

APPENDIX B

EQUATION FOR DIFFUSION-CONTROLLED OXIDATION OF GRAPHITE

Numerous investigators have made theoretical analyses of a diffusion-controlled oxidation process in an aerothermal environment. (See refs. 14, 15, and 16.) While the resulting theoretical equations are different, they lead to the same equation if the Lewis number is assumed to be unity. In reference 16, the Lewis number is assumed to be unity for chemical reactions between a surface and a chemical species outside a laminar boundary layer. Reference 14 gives a theoretical equation in a readily usable form, and with a Lewis number of unity and the rate of formation of pyrolysis products equal to zero, this equation becomes

$$\dot{m}_C = \frac{\lambda c_e}{1 + \lambda \beta c_e}\left(\frac{q}{H_e - H_w}\right) \tag{B1}$$

where $\dot{m}_C$ is the mass loss rate of carbon, λ is the mass of carbon oxidized per unit mass of oxygen consumed, c_e is the mass fraction of oxygen at the boundary-layer edge, β is the blowing coefficient, q is the heat-transfer rate, and H_e and H_w are the enthalpy at the edge of the thermal boundary layer and at the wall, respectively. For the reaction

$$C(s) + \frac{1}{2}O_2(g) \rightarrow CO(g)$$

$\lambda = 3/4$; hence, equation (B1) becomes

$$\dot{m}_C = \frac{0.75 c_e}{1 + 0.75 \beta c_e}\left(\frac{q}{H_e - H_w}\right)$$

or

$$\dot{m}_C = \frac{0.75}{\frac{1}{c_e} + 0.75\beta}\left(\frac{q}{H_e - H_w}\right) \tag{B2}$$

In reference 17, β is evaluated for the case of air injected into a boundary layer of air. For the purpose of the present study it was assumed that the molecular weight of carbon monoxide injected into the boundary layer was sufficiently similar to air to warrant the use of β as evaluated in reference 17:

$$\beta = 1 - \frac{1}{3}N_{Pr,w}^{-0.6} \tag{B3}$$

where $N_{Pr,w}$ is the Prandtl number at wall conditions. For the present study it was assumed that $N_{Pr,w} = 0.71$; hence

$$\beta = 0.59 \tag{B4}$$

Inserting this value of β in equation (B2) results in the following equation for the mass loss rate of graphite:

$$\dot{m}_C = \frac{0.75}{\frac{1}{c_e} + 0.442}\left(\frac{q}{H_e - H_w}\right) \tag{B5}$$

Now

$$\dot{m}_C = \lambda \dot{m}_O = 0.75\dot{m}_O \tag{B6}$$

where $\dot{m}_O$ is the oxygen mass flux. Inserting this value of $\dot{m}_C$ into equation (B5) results in the equation for oxygen mass flux used in the present study:

$$\dot{m}_O = \frac{1}{\frac{1}{c_e} + 0.442}\left(\frac{q}{H_e - H_w}\right) \tag{B7}$$

The heat-transfer coefficient $\frac{q}{H_e - H_w}$ was computed from reference 18.

If CO_2 instead of CO were assumed as the product of the reaction (see ref. 12), then

$$C(s) + O_2(g) \rightarrow CO_2(g) \tag{B8}$$

and $\lambda = 3/8$. Equation (B7) is applicable because the Prandtl number for carbon dioxide is close to that for air, and therefore, equation (B3) for carbon monoxide is valid for carbon dioxide. Theoretical mass loss rates for equation (B8) would be half of those computed by using equation (B6). In this case, the value of $\dot{m}_O$ computed by using equation (B7), in which it was assumed that $\lambda = 3/4$, would be 4.5 percent in error for airstreams, and the error decreases to 1.5 percent as the mass fraction of oxygen in air-nitrogen streams decreases from 0.232 to 0.059.

APPENDIX C

ANALYSIS OF DATA TO DETERMINE THE RATE CONTROLLING MECHANISM

In a chemically controlled reaction, the oxidation rate is (ref. 1)

$$\dot{m}_C = k p_{O,e}^{\alpha} \tag{C1}$$

where $\dot{m}_C$ is the mass loss rate of carbon, k is the specific reaction rate, and $p_{O,e}$ is the partial pressure of oxygen at the outer edge of the concentration boundary layer. Also

$$p_{O,e} = x_e p_{t,2} \tag{C2}$$

where x_e is the mole fraction of oxygen at the outer edge of the concentration boundary layer and $p_{t,2}$ is the total pressure at the outer edge of the concentration boundary layer. The mass fraction of oxygen at the outer edge of the boundary layer can be approximated by

$$c_e \approx x_e \tag{C3}$$

where c_e is the mass fraction of oxygen at the outer edge of the concentration boundary layer. Equation (C3) is valid since the molecular weights of oxygen and air are similar. Combining equations (C3), (C2), and (C1) yields

$$\dot{m}_C \approx k\left(c_e p_{t,2}\right)^{\alpha} \tag{C4}$$

The error introduced by using c_e for x_e ranges from about 10 percent for air to about 13 percent for an air-nitrogen mixture containing 25 percent air by volume. Therefore, it is seen that for a chemically controlled reaction $\dot{m}_C$ is approximately proportional to c_e and $p_{t,2}$ raised to the same power.

In a diffusion-controlled reaction, the oxidation rate is (see eq. (B5), appendix B)

$$\dot{m}_C = \frac{0.75}{\frac{1}{c_e} + 0.442}\left(\frac{q}{H_e - H_w}\right) \tag{C5}$$

where $\frac{q}{H_e - H_w}$ is the heat-transfer coefficient. Since $c_e \leqq 0.232$ for the test conditions of this study,

$$\dot{m}_C \approx 0.75 c_e \left(\frac{q}{H_e - H_w} \right) \tag{C6}$$

It can be shown from reference 18 that, for a modified Newtonian flow, $\frac{q}{H_e - H_w}$ is a weak function of temperature and can be expressed by the following equation:

$$\frac{q}{H_e - H_w} \approx \text{Constant} \times \left(\frac{p_{t,2}}{r} \right)^{1/2} \tag{C7}$$

Therefore, equation (C6) becomes

$$\dot{m}_C \approx \text{Constant} \times c_e \left(\frac{p_{t,2}}{r} \right)^{1/2} \tag{C8}$$

The error introduced in the approximations of equation (C6) ranges from about 10 percent for air to about 2 percent for an air-nitrogen mixture containing 25 percent air by volume. Therefore, it is seen that for a diffusion-controlled reaction $\dot{m}_C$ is approximately proportional to c_e raised to the first power and $p_{t,2}$ raised to the one-half power.

REFERENCES

1. Frank-Kamenetskii, D. A. (N. Thon, trans.): Diffusion and Heat Exchange in Chemical Kinetics. Princeton Univ. Press, 1955.

2. Gulbransen, E. A.; Andrew, K. F.; and Brassart, F. A.: The Oxidation of Graphite at Temperatures of 600° to 1500° C and at Pressures of 2 to 76 Torr of Oxygen. J. Electrochem. Soc., vol. 110, no. 6, June 1963, pp. 476-483.

3. Scala, Sinclaire M.: The Ablation of Graphite in Dissociated Air. Part I: Theory. R62SD72, Missile and Space Div., Gen. Elec. Co., Sept. 1962.

4. Diaconis, N. S.; Gorsuch, P. D.; and Sheridan, R. A.: The Ablation of Graphite in Dissociated Air – Part II: Experiment. Paper No. 62-155, Inst. Aerospace Sci., June 1962.

5. Scala, S. M.; and Gilbert, L. M.: Aerothermochemical Behavior of Graphite at Elevated Temperatures. R63SD89, Missile and Space Div., Gen. Elec. Co., Nov. 1963.

6. Mechtly, E. A.: The International System of Units – Physical Constants and Conversion Factors. NASA SP-7012, 1964.

7. Trout, Otto F., Jr.: Design, Operation, and Testing Capabilities of the Langley 11-Inch Ceramic-Heated Tunnel. NASA TN D-1598, 1963.

8. Mayo, Robert F.; Wells, William L.; and Wallio, Milton A.: A Magnetically Rotated Electric Arc Air Heater Employing a Strong Magnetic Field and Copper Electrodes. NASA TN D-2032, 1963.

9. Schaefer, William T., Jr.: Characteristics of Major Active Wind Tunnels at the Langley Research Center. NASA TM X-1130, 1965.

10. Exton, Reginald J.: Theory and Operation of a Variable Exposure Photographic Pyrometer Over the Temperature Range 1800° to 3600° F (1255° to 2255° K). NASA TN D-2660, 1965.

11. Anon.: The Industrial Graphite Engineering Handbook. Union Carbide Corp., c.1964.

12. Welsh, W. E., Jr.; and Chung, P. M.: A Modified Theory for the Effect of Surface Temperature on the Combustion Rate of Carbon Surfaces in Air. Proc. Heat Transfer Fluid Mech. Inst., Stanford Univ. Press, 1963, pp. 146-159.

13. Williams, David T.: Flow in Pits of Fluid-Dynamic Origin. AIAA J., vol. 1, no. 10, Oct. 1963, pp. 2384-2385.

14. Dow, Marvin B.; and Swann, Robert T.: Determination of Effects of Oxidation on Performance of Charring Ablators. NASA TR R-196, 1964.

15. Eckert, E. R. G. (With Pt. A and Appendix by Robert M. Drake, Jr.): Heat and Mass Transfer. Second ed. of Introduction to the Transfer of Heat and Mass, McGraw-Hill Book Co., Inc., 1959.

16. Lees, Lester: Convective Heat Transfer With Mass Addition and Chemical Reactions. Combustion and Propulsion – Third AGARD Colloquium, M. W. Thring, O. Lutz, J. Fabri, and A. H. Lefebvre, eds., Pergamon Press, 1958, pp. 451-498.

17. Roberts, Leonard: Mass Transfer Cooling Near the Stagnation Point. NASA TR R-8, 1959. (Supersedes NACA TN 4391.)

18. Fay, J. A.; and Riddell, F. R.: Theory of Stagnation Point Heat Transfer in Dissociated Air. J. Aeron. Sci., vol. 25, no. 2, Feb. 1958, pp. 73-85, 121.

TABLE I.- GRAPHITE PROPERTIES

Grade	Density		Maximum grain size		Ash, percent	Forming method
	g/cm^3	kg/m^3	in.	mm		
AGSX	1.67	1670	0.016	0.407	0.13	Extruded
AHDG	1.90	1900	.033	.838	.05	Extruded
ATJ	1.73	1730	.006	.152	.20	Molded

TABLE II.- TEST CONDITIONS

(a) U.S. Customary Units

Test facility	Graphite grade	Model diameter, in.	Nominal Mach number, M	Stagnation pressure, $p_{t,2}$, atm	Stagnation enthalpy, H, Btu/lbm	Cold wall heating rate, q, Btu/ft^2-sec	Mass fraction of oxygen, c_e	Oxygen mass flux, $\dot{m}_O$, lbm/ft^2-sec
Langley 20-inch hypersonic arc-heated tunnel	ATJ	0.375	6	0.0606 to 0.197	1809 to 4080	237 to 430	0.117 to 0.232	0.0167 to 0.0248
	AHDG	0.375, 1	6	0.0606 to 0.197	1809 to 4080	237 to 430	0.117 to 0.232	0.0127 to 0.0248
	AGSX	0.375	6	0.0606 to 0.197	1809 to 4080	255 to 430	0.117 to 0.232	0.0167 to 0.0248
Arc-heated materials jet at the Langley Research Center	ATJ	0.375, .5	2	6.38			0.059 to 0.232	0.0319 to 0.148
	AHDG	0.375, .5	2	6.38 to 8.28	910 to 1063	653 to 812	0.059 to 0.232	0.0319 to 0.166
	AGSX	0.5	2	6.38			0.059 to 0.232	0.0319 to 0.128
Langley 11-inch ceramic-heated tunnel	ATJ	0.375, .5	2	5.17 to 7.42	643 to 1078	352 to 695	0.232	0.119 to 0.143
	AHDG	0.375, .5, 1	2	5.17 to 7.50	729 to 1078	303 to 810	0.232	0.086 to 0.171
	AGSX	0.5, 1	2	5.17 to 7.50	595 to 1079	291 to 745	0.232	0.086 to 0.143

(b) SI Units

Test facility	Graphite grade	Model diameter, cm	Nominal Mach number, M	Stagnation pressure, $p_{t,2}$, N/m^2	Stagnation enthalpy, H, MJ/kg	Cold wall heating rate, q, MW/m^2	Mass fraction of oxygen, c_e	Oxygen mass flux, $\dot{m}_O$, kg/m^2-s
Langley 20-inch hypersonic arc-heated tunnel	ATJ	0.953	6	6.12 to 19.9×10^3	4.20 to 9.47	2.69 to 4.88	0.117 to 0.232	0.0815 to 0.1210
	AHDG	0.953, 2.54	6	6.12 to 19.9×10^3	4.20 to 9.47	2.69 to 4.88	0.117 to 0.232	0.0620 to 0.1210
	AGSX	0.953	6	6.12 to 19.9×10^3	4.20 to 9.47	2.89 to 4.88	0.117 to 0.232	0.0815 to 0.1210
Arc-heated materials jet at the Langley Research Center	ATJ	0.953, 1.27	2	6.50×10^5			0.059 to 0.232	0.1557 to 0.722
	AHDG	0.953, 1.27	2	6.50 to 8.39×10^5	2.11 to 2.47	7.41 to 9.22	0.059 to 0.232	0.1557 to 0.811
	AGSX	1.27	2	6.50×10^5			0.059 to 0.232	0.1557 to 0.623
Langley 11-inch ceramic-heated tunnel	ATJ	0.953, 1.27	2	5.22 to 7.50×10^5	1.49 to 2.50	4.00 to 7.93	0.232	0.581 to 0.698
	AHDG	0.953, 1.27, 2.54	2	5.22 to 7.60×10^5	1.69 to 2.50	3.44 to 9.19	0.232	0.420 to 0.834
	AGSX	1.27, 2.54	2	5.22 to 7.60×10^5	1.38 to 2.50	3.32 to 8.49	0.232	0.420 to 0.698

TABLE III.- TEST PARAMETERS AND RESULTS FOR ATJ GRAPHITE MODELS

(a) U.S. Customary Units

Test facility and Mach number	Model diameter, in.	Stagnation pressure, $P_{t,2}$, atm	Stagnation enthalpy, Btu/lbm	Cold wall heating rate, Btu/ft^2-sec	Mass fraction of oxygen	Oxygen mass flux, lbm/ft^2-sec	Mass loss rate of graphite, lbm/ft^2-sec	Surface temperature at stagnation point, $^\circ$R	Model shape (*)	Run time, sec
Langley 20-inch hypersonic arc-heated tunnel (Mach number = 6)	0.375	0.0606	1809	371	0.232	0.0167	0.0113	3710	R	120
		.0606	1809	340		.0167	.0117	3760		
		.101	2605	282		.0210	.0075	3210		
		.197	4080	237		.0248	.0126	3200		
		.197	4080	255		.0248	.0106	3250		
		.0606	1809	400		.0167	.0102	3840		
				428			.0115	3790		
				412			.0096	3650		
		.1285		430	.117	.0171	.0098	3600		75
				328	.117	.0171	.0077	3220		89
					.170	.0204	.0076	3245		101
				315	.232	.0224	.0091	3280		120
Arc-heated materials jet at the Langley Research Center (Mach number = 2)	0.5	6.38			0.059	0.0319	0.0154	3840	R	30
							.0153	3410		
							.0199	3690		
					.117	.0638	.0351	3545		
							.0324	3610		
							.0343	3220		
					.170	.0970	.0468	3835		
							.0414	3470		27
							.0579	3430		30
							.0526	3640		
					.232	.1276	.0616	3710		
							.0519	4000		
							.0580	3975		60
							.0737	3680		30
							.0723	3675		60
	.375					.148	.0745	4130		41
Langley 11-inch ceramic-heated tunnel (Mach number = 2)	0.375	5.17	709	400	0.232	0.140	0.0627	3670	R	113
			643	352			.0702	3610		92
			709	400			.0735	3460		158
	.5		1078	580		.119	.0620	3800		30
				580		.119	.0605			60
		7.42		695		.143	.0679			30

(b) SI Units

Test facility and Mach number	Model diameter, cm	Stagnation pressure, $P_{t,2}$, N/m^2	Stagnation enthalpy, MJ/kg	Cold wall heating rate, MW/m^2	Mass fraction of oxygen	Oxygen mass flux, kg/m^2-s	Mass loss rate of graphite, kg/m^2-s	Surface temperature at stagnation point, $^\circ$K	Model shape (*)	Run time, sec
Langley 20-inch hypersonic arc-heated tunnel (Mach number = 6)	0.95	6.12×10^3	4.20	4.21	0.232	0.0815	0.0551	2060	R	120
		6.12	4.20	3.86		.0815	.0571	2090		
		10.20	6.04	3.20		.1025	.0366	1790		
		19.90	9.47	2.69		.1210	.0615	1780		
		19.90	9.47	2.89		.1210	.0517	1810		
		6.12	4.20	4.54		.0815	.0498	2140		
				4.86			.0561	2110		
				4.68			.0468	2030		
		13.00		4.88	.117	.0834	.0478	2000		75
				3.72	.117	.0834	.0376	1790		89
					.170	.0996	.0371	1800		101
				3.58	.232	.1093	.0444	1820		120
Arc-heated materials jet at the Langley Research Center (Mach number = 2)	1.27	6.50×10^5			0.059	0.1557	0.0752	2140	R	30
							.0747	1900		
							.0971	2050		
					.117	.3113	.1713	1970		
							.1581	2010		
							.1674	1790		
					.170	.4734	.2284	2130		
							.2020	1930		27
							.2826	1910		30
							.2567	2020		
					.232	.6227	.3006	2060		
							.2533	2220		
							.2830	2210		60
							.3597	2050		30
							.3528	2040		60
	.95					.7222	.3636	2300		41
Langley 11-inch ceramic-heated tunnel (Mach number = 2)	0.95	5.22×10^5	1.64	4.54	0.232	0.6832	0.3060	2040	R	113
			1.49	4.00			.3426	2010		92
			1.64	4.54			.3587	1920		158
	1.27		2.50	6.61		.5807	.3026	2110		30
				6.61		.5807	.2952			60
		7.50		7.93		.6978	.3314			30

*The letter R denotes round model shape.

TABLE IV.- TEST PARAMETERS AND RESULTS FOR AHDG GRAPHITE MODELS

(a) U.S. Customary Units

Test facility and Mach number	Model diameter, in.	Stagnation pressure, $p_{t,2}$, atm	Stagnation enthalpy, Btu/lbm	Cold wall heating rate, Btu/ft^2-sec	Mass fraction of oxygen	Oxygen mass flux, lbm/ft^2-sec	Mass loss rate of graphite, lbm/ft^2-sec	Surface temperature at stagnation point, $^\circ$R	Model shape (*)	Run time, sec
Langley 20-inch	0.375	0.0606	1809	371	0.232	0.0167	0.0124	3710	R	120
hypersonic arc-		.0606	1809			.0167	.0108	3760		
heated tunnel		.101	2605	282		.0210	.0093	3160		
(Mach number = 6)		.197	4080	237		.0248	.0087	3000		
		.197	4080	255		.0248	.0111	3110		
		.0606	1809	400		.0167	.0112	3840		
		↓	↓	412		↓	.0099	3670		
		↓	↓	428	↓	↓	.0099	3280		
		.1285		430	.117	.0171	.0094	3350		↓
		↓		328	.117	.0171	.0052	2770		89
		↓			.170	.0204	.0064	3140		101
		↓		315	.232	.0224	.0086	2975		120
	1	.171	3700	240	.232	.0127	.0089	3430	↓	180
Arc-heated mate-	0.5	6.38			0.059	0.0319	0.0158	3470	R	30
rials jet at the		↓			↓	↓	.0261	3500	R	30
Langley Research		↓			↓	↓	.0180	3770	S	60
Center		↓			↓	↓	.0210	3370	R	90
(Mach number = 2)		↓			.117	.0638	.0511	3660	↓	30
		↓			.117	.0638	.0406	3520	↓	↓
		↓			.170	.0970	.0641	3700	S	↓
		↓			↓	↓	.0527	3700	↓	↓
		↓			↓	↓	.0548	3535	↓	↓
		↓			.232	.1276	.0760	↓	↓	20
		↓			↓	↓	.0815	↓	↓	30
		↓			↓	↓	.0914	3585	↓	↓
		↓			↓	↓	.0623	3640	↓	↓
		↓			↓	↓	.0666	↓	D	60
	.375	8.28	1063	812	.059	.0471	.0171	2845	S	30
	↓	7.78	958	691	.117	.0900	.0325	3110	S	↓
	↓	8.26	987	742	.170	.1357	.0510	3250	R	↓
	↓	7.83	910	653	.232	.1662	.0660	3840	D	↓
	↓	6.38	↓	↓	.059	.0369	.0177	3660	R	↓
	↓	↓	↓	↓	.117	.0739	.0370	3770	S	↓
	↓	↓	↓	↓	.170	.1108	.0492	3860	S	↓
Langley 11-inch	1	5.17	837	303	0.232	0.0860	0.0362	3570	S	102
ceramic-heated	↓	5.17	1078	416	↓	.0880	.0433	3430	R	53
tunnel	↓	7.50	1078	497	↓	.1050	.0477	3685	S	55
(Mach number = 2)	↓	7.50	837	362	↓	.1030	.0756	3780	↓	60
	.375	5.17	1078	680	↓	.1430	.0620	3695	↓	37
	↓	↓	↓	580	↓	.1190	.0631	↓	↓	30
	↓	↓	↓	580	↓	.1190	.0596	↓	↓	↓
	↓	6.05	↓	630	↓	.1290	.0603	↓	↓	↓
	1	7.50	729	305	↓	.1020	.1930	4060	D	106
	↓	↓	837	362	↓	.1030	.1040	3630	D	60
	↓	↓	837	362	↓	.1030	.0842	3780	S	↓
	↓	↓	1078	497	↓	.1050	.0600	3930	D	↓
	.5	↓	↓	704	↓	.1460	.1420	3990	↓	50
	↓	↓	↓	704	↓	↓	.1000	3975	↓	25
	↓	↓	837	514	↓	↓	.1670	3650	↓	54
	.375	↓	837	592	↓	.1680	.1620	3860	↓	43
	.375	↓	1078	810	↓	.1710	.0760	3925	↓	20

*The letter R denotes round model shape, the letter S denotes stagnation region intact, and the letter D denotes distorted model shape.

TABLE IV.- TEST PARAMETERS AND RESULTS FOR AHDG GRAPHITE MODELS – Concluded

(b) SI Units

Test facility and Mach number	Model diameter, cm	Stagnation pressure, $p_{t,2}$, N/m^2	Stagnation enthalpy, MJ/kg	Cold wall heating rate, MW/m^2	Mass fraction of oxygen	Oxygen mass flux, kg/m^2-s	Mass loss rate of graphite, kg/m^2-s	Surface temperature at stagnation point, °K	Model shape (*)	Run time, sec
Langley 20-inch hypersonic arc-heated tunnel (Mach number = 6)	0.95	6.12×10^3	4.20	4.21	0.232	0.0815	0.0605	2060	R	120
		6.12	4.20			.0815	.0527	2090		
		10.20	6.04	3.20		.1025	.0454	1760		
		19.90	9.47	2.69		.1210	.0425	1670		
		19.90	9.47	2.89		.1210	.0542	1730		
		6.12	4.20	4.54		.0815	.0547	2140		
				4.68			.0483	2040		
				4.86			.0483	1820		
		13.00		4.88	.117	.0834	.0459	1860		
				3.72	.117	.0834	.0254	1540		89
					.170	.0996	.0312	1750		101
				3.58	.232	.1093	.0420	1650		120
	2.54	17.30	8.58	2.74	.232	.0620	.0434	1910		180
Arc-heated materials jet at the Langley Research Center (Mach number = 2)	1.27	6.50×10^5			0.059	0.1557	0.0771	1930	R	30
							.1274	1950	R	30
							.0878	2100	S	60
							.1025	1870	R	90
					.117	.3113	.2494	2040		30
					.117	.3113	.1981	1960		
					.170	.4734	.3128	2060	S	
							.2572	2060		
							.2674	1970		
					.232	.6227	.3709			20
							.3977			30
							.4460	1990		
							.3040	2020		
							.3250		D	60
	.95	8.39	2.47	9.22	.059	.2298	.0834	1580	S	30
		7.88	2.22	7.84	.117	.4392	.1586	1730	S	
		8.34	2.29	8.42	.170	.6622	.2489	1810	R	
		7.91	2.11	7.41	.232	.8111	.3221	2140	D	
		6.50			.059	.1801	.0864	2040	R	
					.117	.3606	.1806	2100	S	
					.170	.5407	.2401	2150	S	
Langley 11-inch ceramic-heated tunnel (Mach number = 2)	2.54	5.22×10^5	1.94	3.44	0.232	0.4197	0.1767	1990	S	102
		5.22	2.50	4.72		.4294	.2113	1910	R	53
		7.60	2.50	5.64		.5124	.2328	2050	S	55
		7.60	1.94	4.11		.5026	.3689	2100		60
	.95	5.22	2.50	7.72		.6978	.3026	2050		37
				6.61		.5807	.3079			30
				6.61		.5807	.2908			
		6.11		7.18		.6295	.2943			
	2.54	7.60	1.69	3.46		.4978	.9418	2260	D	106
			1.94	4.11		.5026	.5075	2020	D	60
			1.94	4.11		.5026	.4109	2100	S	
			2.50	5.64		.5124	.2928	2190	D	
	1.27			7.99		.7125	.6930	2220		50
				7.99			.4880	2210		25
			1.94	5.83			.8150	2030		54
	.95		1.94	6.72		.8198	.7906	2150		43
	.95		2.50	9.19		.8345	.3709	2180		20

*The letter R denotes round model shape, the letter S denotes stagnation region intact, and the letter D denotes distorted model shape.

TABLE V.- TEST PARAMETERS AND RESULTS FOR AGSX GRAPHITE MODELS

(a) U.S. Customary Units

Test facility and Mach number	Model diameter, in.	Stagnation pressure, $p_{t,2}$, atm	Stagnation enthalpy, Btu/lbm	Cold wall heating rate, Btu/ft^2-sec	Mass fraction of oxygen	Oxygen mass flux, lbm/ft^2-sec	Mass loss rate of graphite, lbm/ft^2-sec	Surface temperature at stagnation point, °R	Model shape (*)	Run time, sec
Langley 20-inch hypersonic arc-heated tunnel (Mach number = 6)	0.375	0.0606	1809	371	0.232	0.0167	0.0110	3660	R	120
		.0606	1809	340		.0167	.0112	3760		
		.101	2605	282		.0210	.0078	3160		
		.197	4080	255		.0248	.0065	2950		
		.0606	1809	400		.0167	.0109	3730		
				412			.0094	3600		
				428			.0103	3420		
		.1285		430	.117	.0171	.0086	3110		
				328	.117	.0171	.0047	2710		
					.170	.0204	.0063	2900		101
				315	.232	.0224	.0069	2940		120
Arc-heated materials jet at the Langley Research Center (Mach number = 2)	0.5	6.38			0.059	0.0319	0.0186	3595	S	30
					.059	.0319	.0226	3460	R	
					.117	.0638	.0432	3990	D	
							.0423	3800		
							.0515	3625		
					.170	.0970	.0623	3740		
							.0751			
							.0808	3680		
					.232	.1276	.1240	3640		
							.0927			
							.0695	3730		
							.0673	3640	R	
							.0661	3670	R	
Langley 11-inch ceramic-heated tunnel (Mach number = 2)	1	5.63	842	473	0.232	0.0860	0.1397	4190	D	78
		5.63	595	291		.0860	.0800	4100		126
		7.50	685	419		.1020	.1910	4000		60
			732	457		.1020	.1850	4010		64
			842	543		.1030	.1570	3725		60
			1079	745		.1050	.1270	3860		60
	.5	5.17	1078	580		.1190	.0569		S	30
		6.05		630		.1290	.0671			
		7.42		695		.1430	.0726			

(b) SI Units

Test facility and Mach number	Model diameter, cm	Stagnation pressure, $p_{t,2}$, N/m^2	Stagnation enthalpy, MJ/kg	Cold wall heating rate, MW/m^2	Mass fraction of oxygen	Oxygen mass flux, kg/m^2-s	Mass loss rate of graphite, kg/m^2-s	Surface temperature at stagnation point, °K	Model shape (*)	Run time, sec
Langley 20-inch hypersonic arc-heated tunnel (Mach number = 6)	0.95	6.12×10^3	4.20	4.21	0.232	0.0815	0.0537	2035	R	120
		6.12	4.20	3.86		.0815	.0547	2090		
		10.20	6.04	3.20		.1025	.0381	1760		
		19.90	9.47	2.89		.1210	.0317	1640		
		6.12	4.20	4.54		.0815	.0532	2070		
				4.68			.0459	2000		
				4.86			.0503	1900		
		13.00		4.88	.117	.0635	.0420	1730		
				3.72	.117	.0835	.0229	1510		
					.170	.0996	.0307	1610		101
				3.58	.232	.1093	.0337	1640		120
Arc-heated materials jet at the Langley Research Center (Mach number = 2)	1.27	6.50×10^5			0.059	0.1557	0.0908	2000	S	30
					.059	.1557	.1103	1920	R	
					.117	.3113	.2108	2220	D	
							.2064	2110		
							.2513	2020		
					.170	.4734	.3040	2080		
							.3665			
							.3943	2050		
					.232	.6227	.6051	2020		
							.4524			
							.3392	2070		
							.3284	2020	R	
							.3226	2040	R	
Langley 11-inch ceramic-heated tunnel (Mach number = 2)	2.54	5.69×10^5	1.95	5.40	0.232	0.4197	0.6817	2330	D	78
		5.69	1.38	3.32		.4197	.3904	2280		126
		7.60	1.59	4.78		.4978	.9321	2220		60
			1.70	5.21		.4978	.9028	2230		64
			1.95	6.20		.5026	.7662	2070		60
			2.50	8.49		.5124	.6198	2150		60
	1.27	5.22		6.61		.5807	.2777		S	30
		6.11		7.18		.6295	.3274			
		7.49		7.93		.6978	.3543			

*The letter R denotes round model shape, the letter S denotes stagnation region intact, and the letter D denotes distorted model shape.

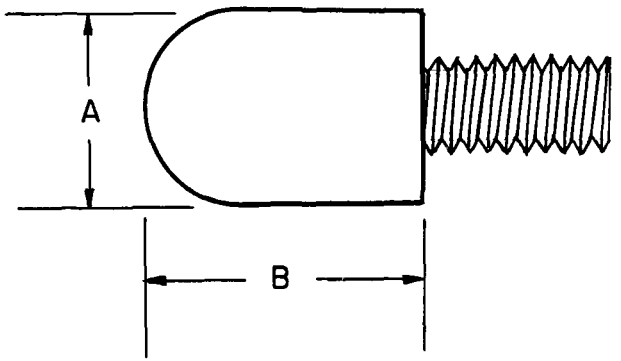

A		B	
in.	cm	in.	cm
0.375	0.953	0.563	1.429
0.500	1.270	0.750	1.905
1.000	2.540	1.500	3.810

(a) Models of AHDG and AGSX graphite.

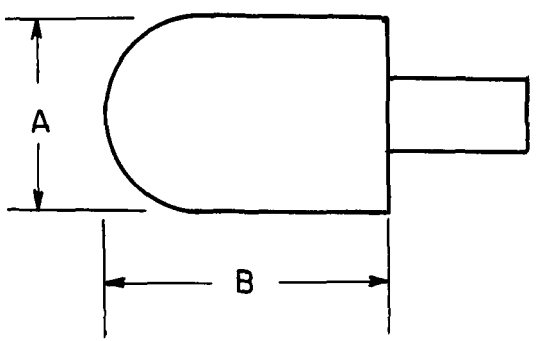

A		B	
in.	cm	in.	cm
0.375	0.953	0.750	1.905
0.500	1.270	0.750	1.905

(b) Models of ATJ graphite.

Figure 1.- Construction details of hemispherical graphite models.

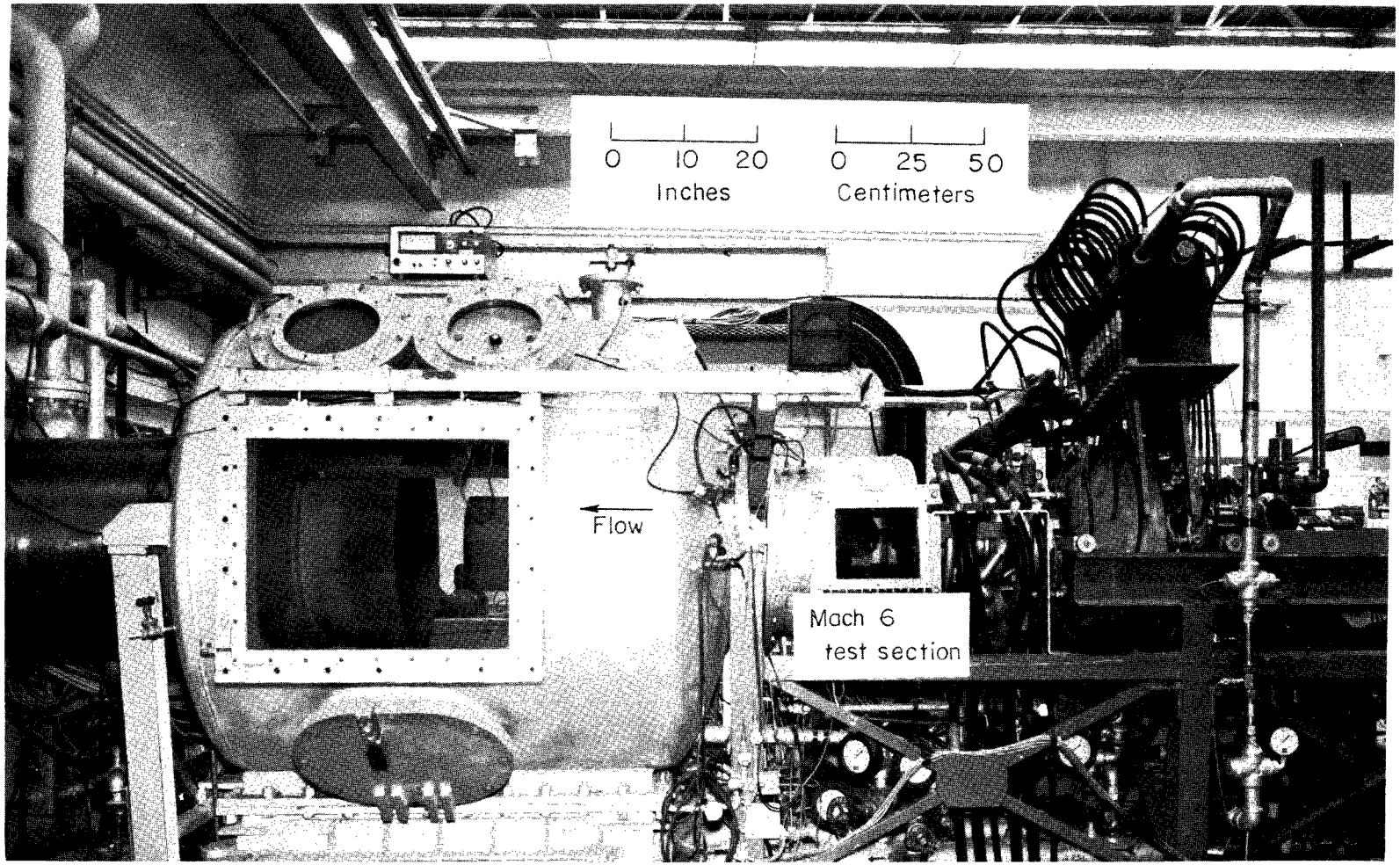

Figure 2.- Photograph of Langley 20-inch hypersonic arc-heated tunnel. L-64-10,808

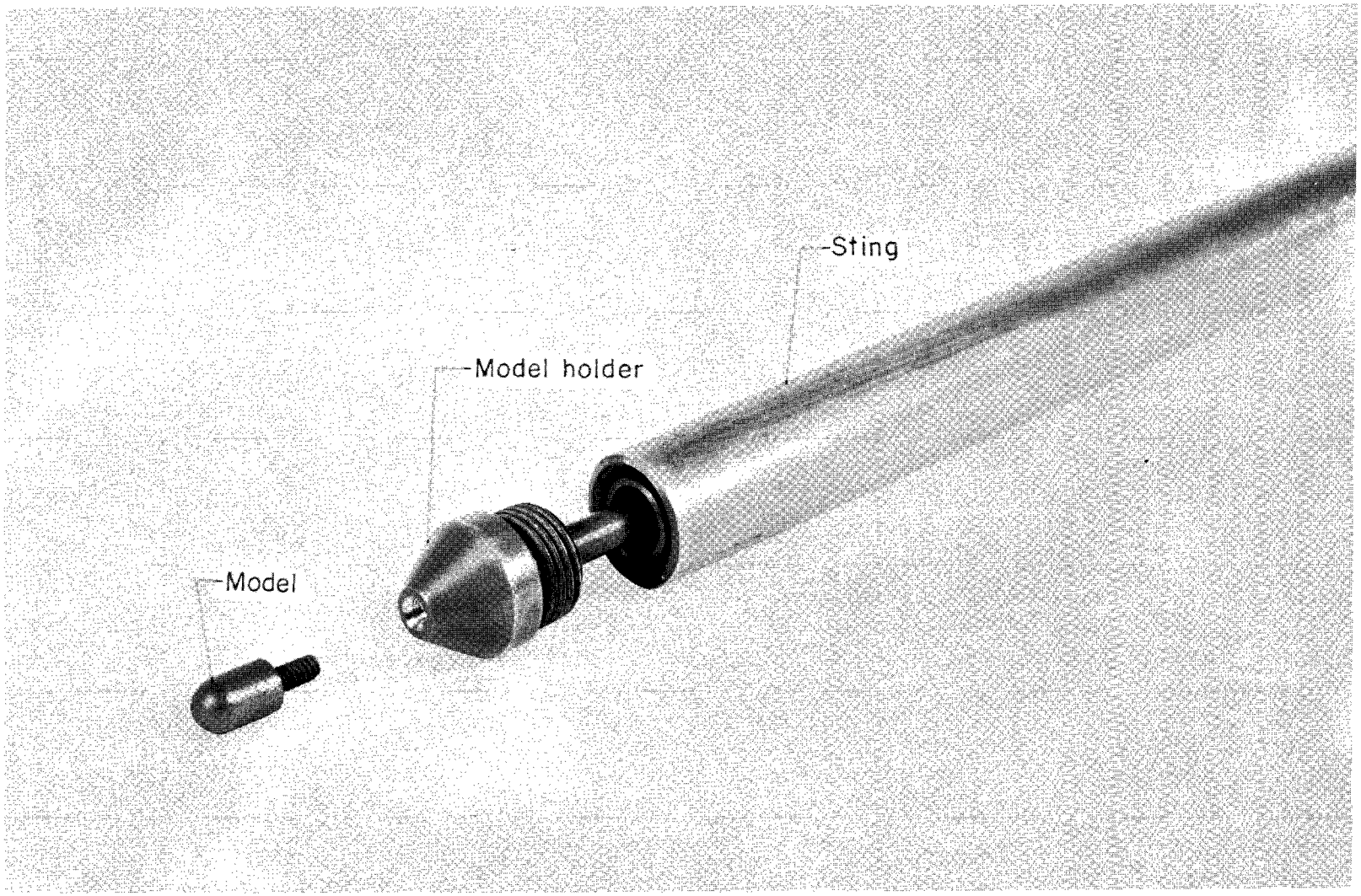

(a) 0.375-inch-diameter (0.953-cm) model. L-64-799.1

Figure 3.- Photographs of model, model holders, and water-cooled sting assemblies.

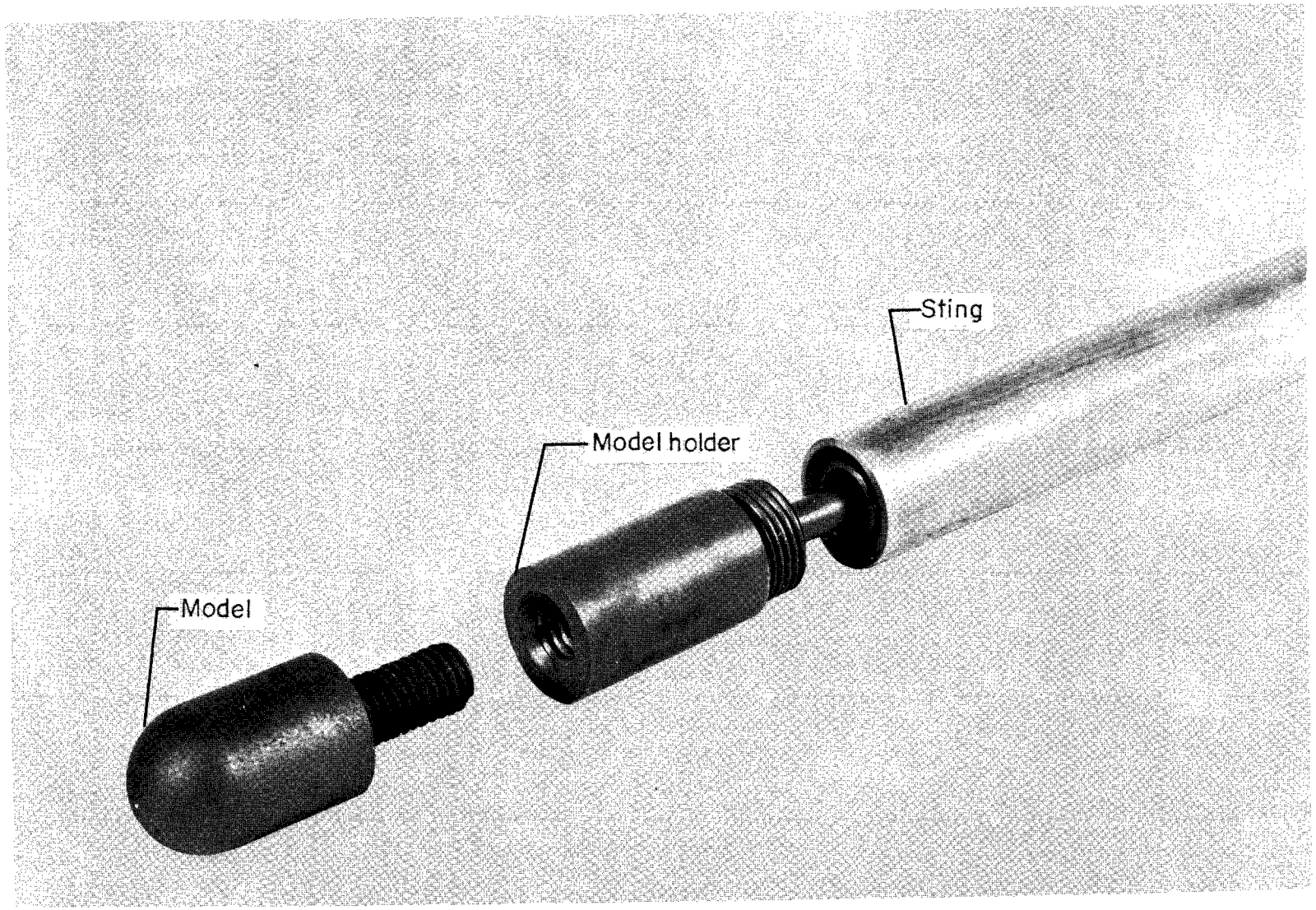

(b) 1-inch-diameter (2.54-cm) model. L-64-798.1

Figure 3.- Continued.

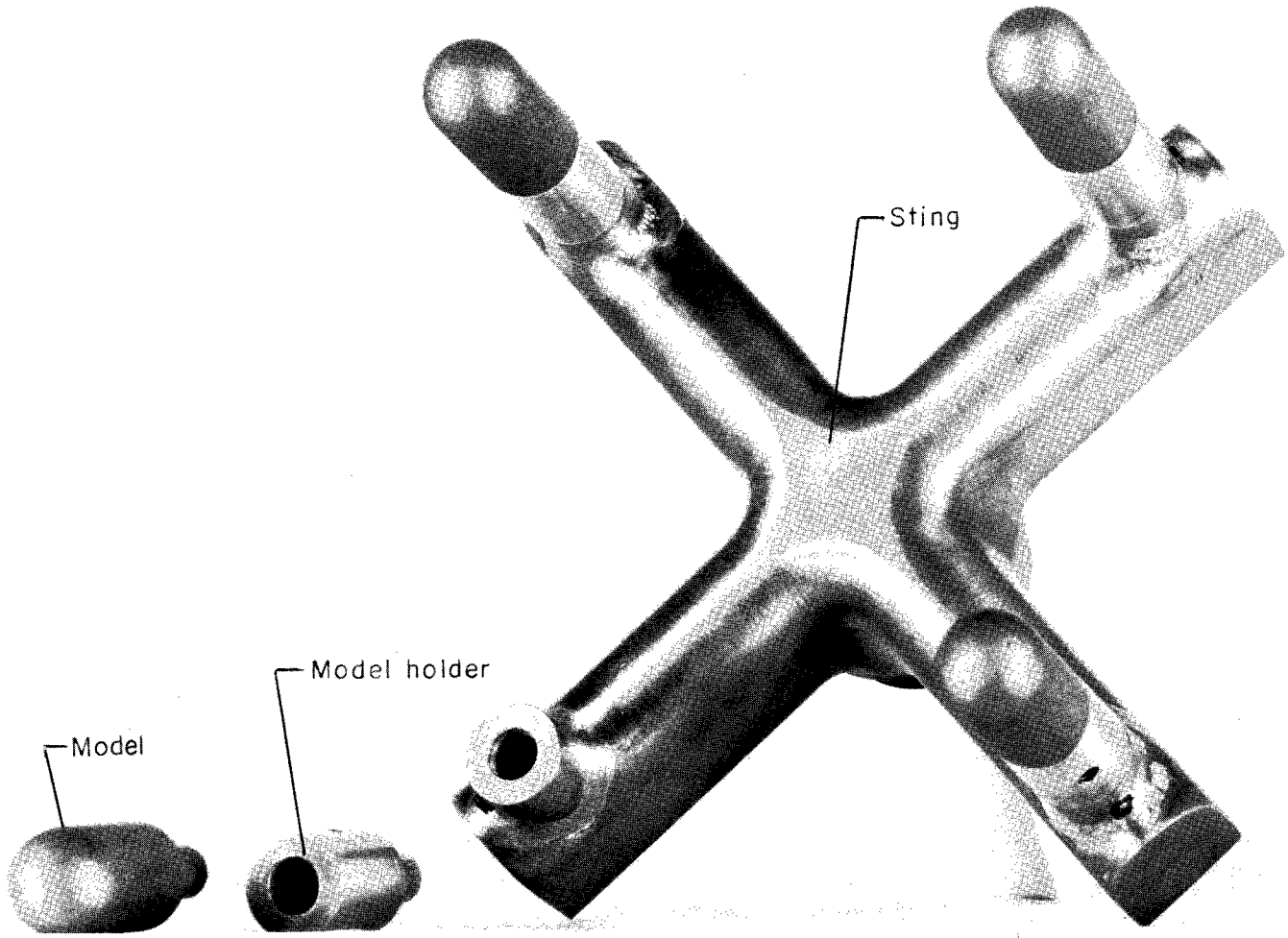

(c) Four-model holder for 0.375-inch-diameter (0.953-cm) models. L-65-4673.1

Figure 3.- Concluded.

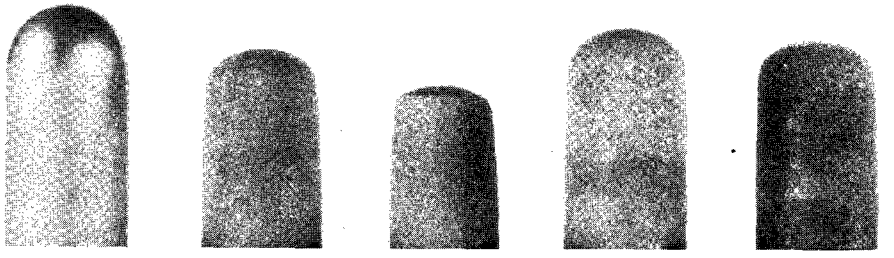

$\dot{m}_O$, lbm/ft^2-sec (kg/m^2-s)	Untested	0.0167 (0.0815)	0.0167 (0.0815)	0.0210 (0.1025)	0.0248 (0.1210)
t, sec		120	240	120	120
T_w, °R (°K)		3760 (2090)	3745 (2080)	3210 (1785)	3250 (1810)
$p_{t,2}$, atm		0.0606	0.0606	0.101	0.197

(a) 0.375-inch-diameter (0.953-cm) models exposed to low stagnation pressures; oxygen mass fraction c_e = 0.232.

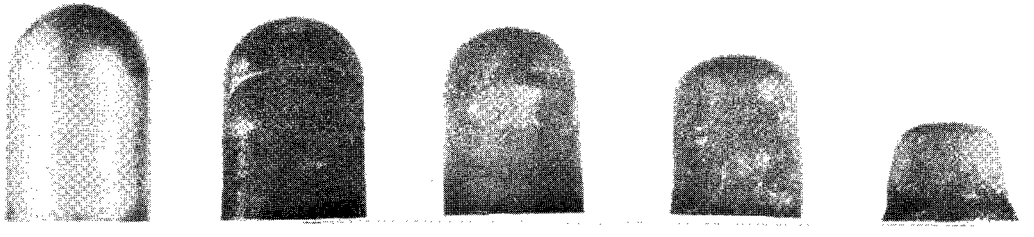

$\dot{m}_O$, lbm/ft^2-sec (kg/m^2-s)	Untested	0.0319 (0.1558)	0.0638 (0.312)	0.1276 (0.622)	0.1276 (0.622)
t, sec		30	30	30	60
T_w, °R (°K)		3840 (2130)	3835 (2130)	4000 (2220)	3975 (2210)
c_e		0.059	0.117	0.232	0.232

(b) 0.5-inch-diameter (1.27-cm) models exposed to high stagnation pressure of 6.4 atm. L-66-1094

Figure 4.- Models of ATJ graphite exposed to wide range of oxygen mass flux.

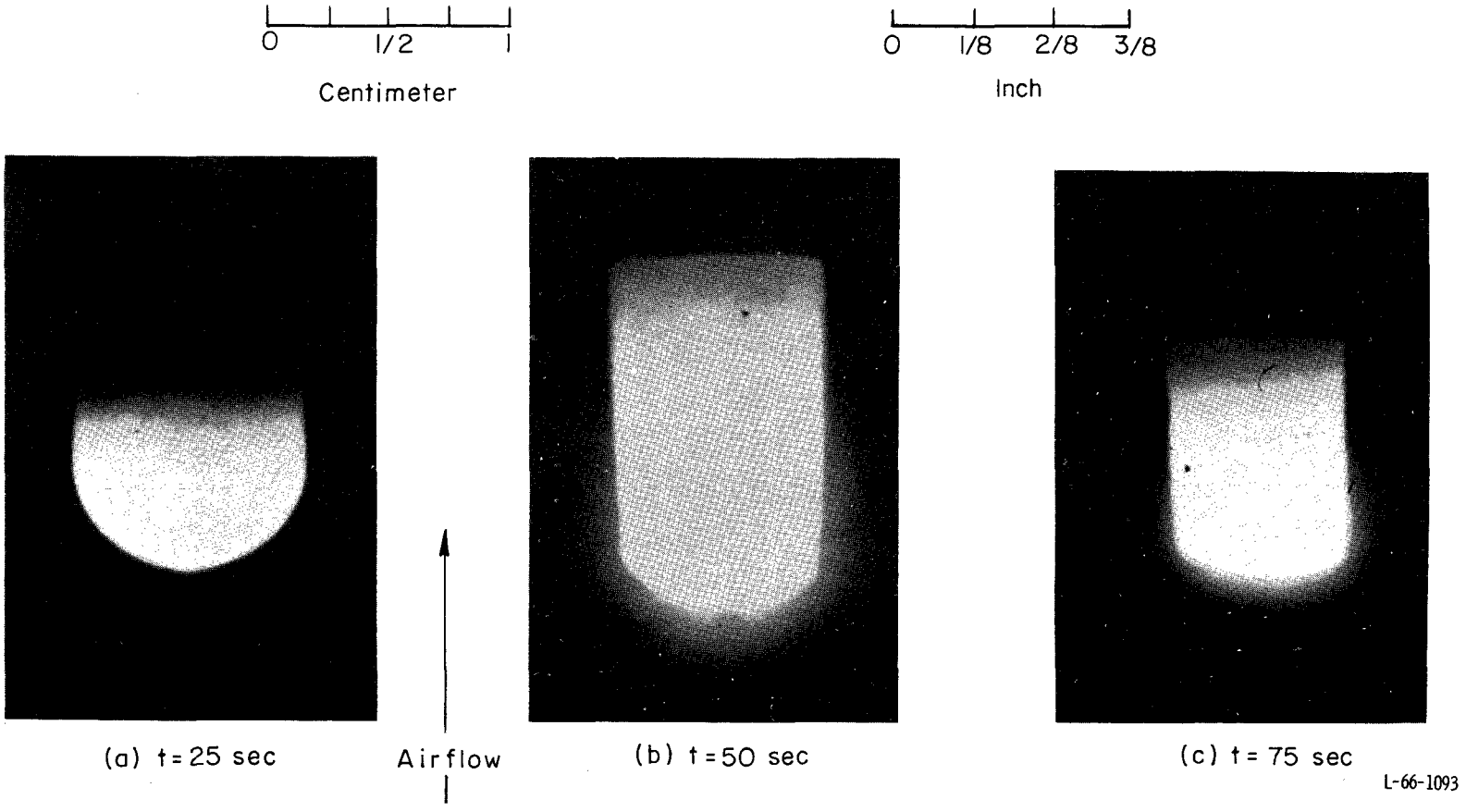

Figure 5.- Typical effect of exposing 0.375-inch-diameter (0.953-cm) ATJ graphite model to high oxygen mass flux for a long run time. $\dot{m}_O$ = 0.140 lbm/ft^2-sec (0.683 kg/m^2-s); $p_{t,2}$ = 5.17 atm; Total exposure time = 113 sec; c_e = 0.232; Equilibrium T_w = 3890^0 R (2160^0 K).

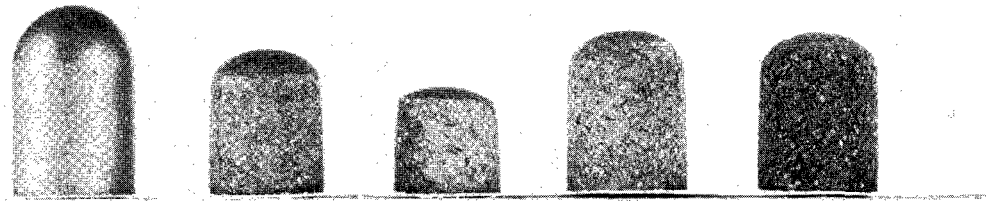

$\dot{m}_O$, lbm/ft^2-sec (kg/m^2-s)	Untested	0.0167 (0.0815)	0.0167 (0.0815)	0.0210 (0.1025)	0.0248 (0.1210)
t, sec		120	140	120	120
T_w, °R (°K)		3760 (2090)	3755 (2085)	3160 (1760)	3110 (1730)
$p_{t,2}$, atm		0.0606	0.0606	0.101	0.197

(a) 0.375-inch-diameter (0.953-cm) models exposed to low stagnation pressures; oxygen mass fraction c_e = 0.232.

$\dot{m}_O$, lbm/ft^2-sec (kg/m^2-s)	Untested	Nitrogen	0.0319 (0.1558)	0.0638 (0.312)	0.1276 (0.622)
t, sec		30	60	59	60
T_w, °R (°K)		3490 (1940)	3770 (2095)	3835 (2130)	
c_e		0	0.059	0.117	0.232
Model	1	2	3	4	5

(b) 0.5-inch-diameter (1.27-cm) models exposed to high stagnation pressure of 6.4 atm.

L-66-1092

Figure 6.- Models of AHDG graphite exposed to wide range of oxygen mass flux.

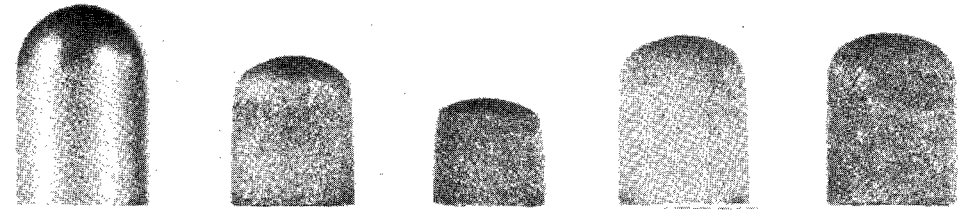

$\dot{m}_O$, lbm/ft^2-sec (kg/m^2-s)	Untested	0.0167 (0.0815)	0.0167 0.0815	0.0210 (0.1025)	0.0248 (0.1210)
t, sec		120	240	120	120
T_w, °R (°K)		3760 (2090)	3665 (2030)	3160 (1760)	3110 (1730)
$p_{t,2}$, atm		0.0606	0.0606	0.101	0.197

(a) 0.375-inch-diameter (0.953-cm) models exposed to low stagnation pressures; oxygen mass fraction c_e = 0.232.

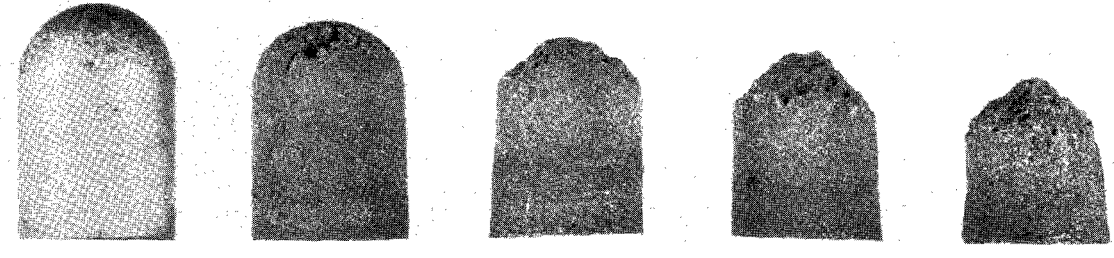

$\dot{m}_O$, lbm/ft^2-sec (kg/m^2-s)	Untested	0.0319 (0.1558)	0.0638 (0.312)	0.1276 (0.622)	0.1276 (0.622)
t, sec		30	30	30	60
T_w, °R (°K)		3595 (2000)	3800 (2110)	3740 (2080)	3710 (2060)
c_e		0.059	0.117	0.170	0.232
Model	1	2	3	4	5

(b) 0.5-inch-diameter (1.27-cm) models exposed to high stagnation pressure of 6.4 atm. L-66-1091

Figure 7.- Models of AGSX graphite exposed to wide range of oxygen mass flux.

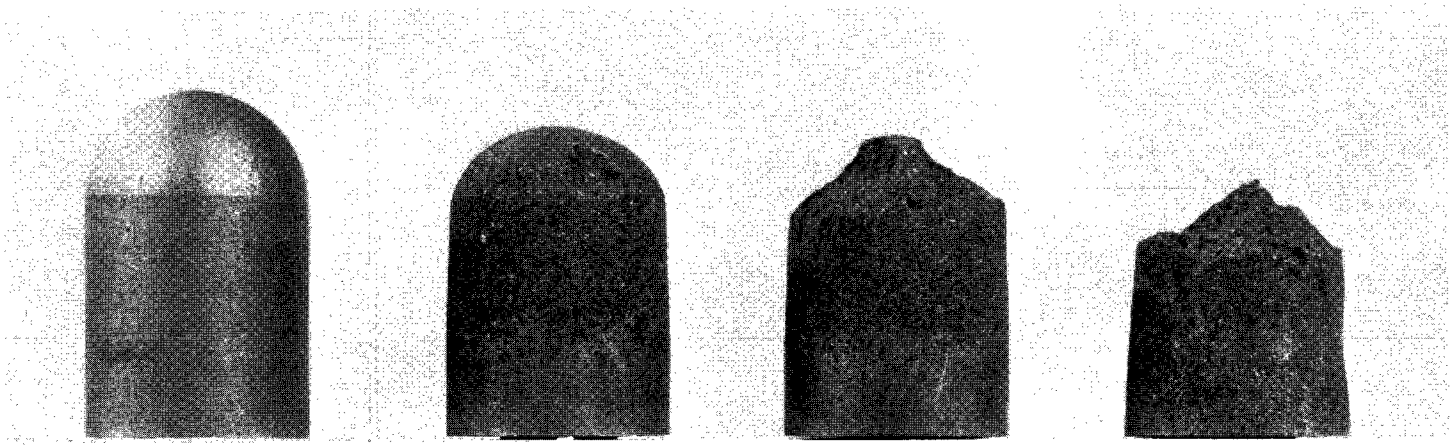

$\dot{m}_O$, lbm/ft^2-sec (kg/m^2-s)	Untested	0.088 (0.429)	0.103 (0.502)	0.105 (0.512)
t, sec		60	60	60
T_w, °R (°K)		3430 (1910)	3780 (2100)	3930 (2185)
$p_{t,2}$, atm		5.17	7.50	7.50
c_e		0.232	0.232	0.232

Figure 8.- 1-inch-diameter (2.54-cm) AHDG graphite models exposed to high stagnation pressures and high oxygen mass flux. L-66-1090.1

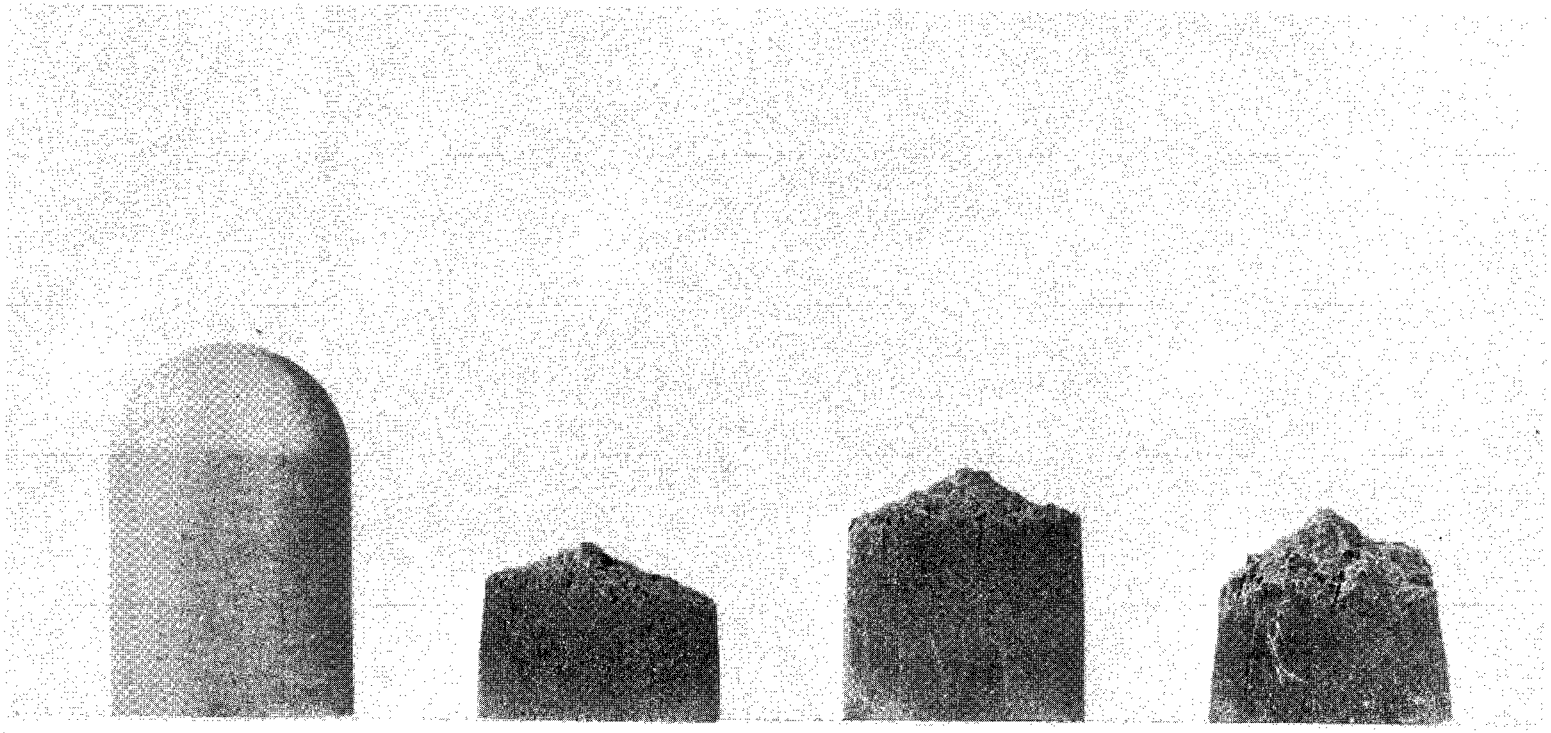

	Untested			
$\dot{m}_O$, lbm/ft^2-sec		0.102	0.103	0.105
(kg/m^2-s)		(0.497)	(0.502)	(0.512)
t, sec		60	60	60
T_w, °R (°K)		4000 (2220)	3725 (2070)	3860 (2145)
$p_{t,2}$, atm		7.50	7.50	7.50
c_e		0.232	0.232	0.232

Figure 9.- 1-inch-diameter (2.54-cm) AGSX graphite models exposed to high stagnation pressure and high oxygen mass flux. L-64-803.1

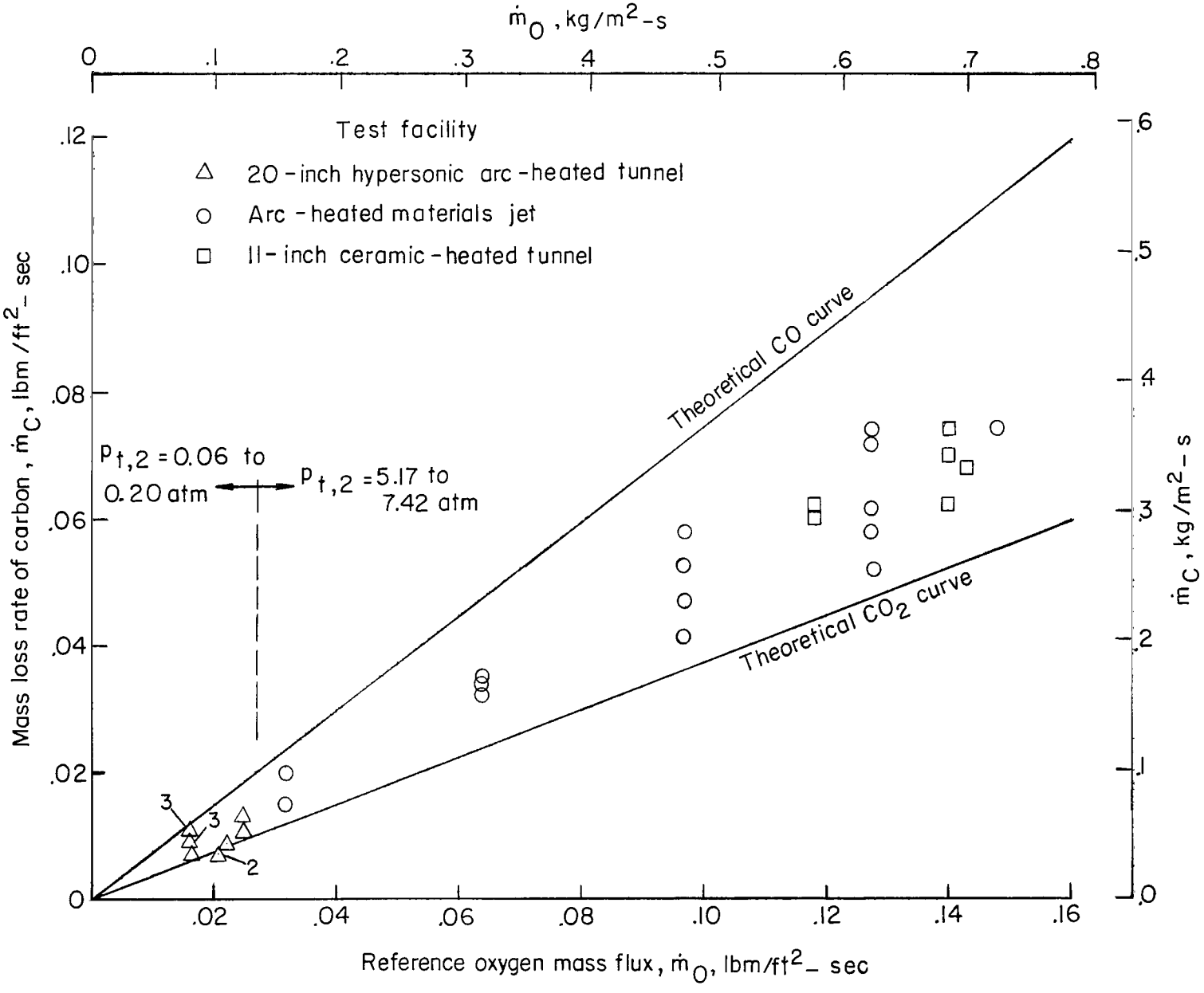

Figure 10.- Comparison of oxidation rates of ATJ graphite with theoretical curves.

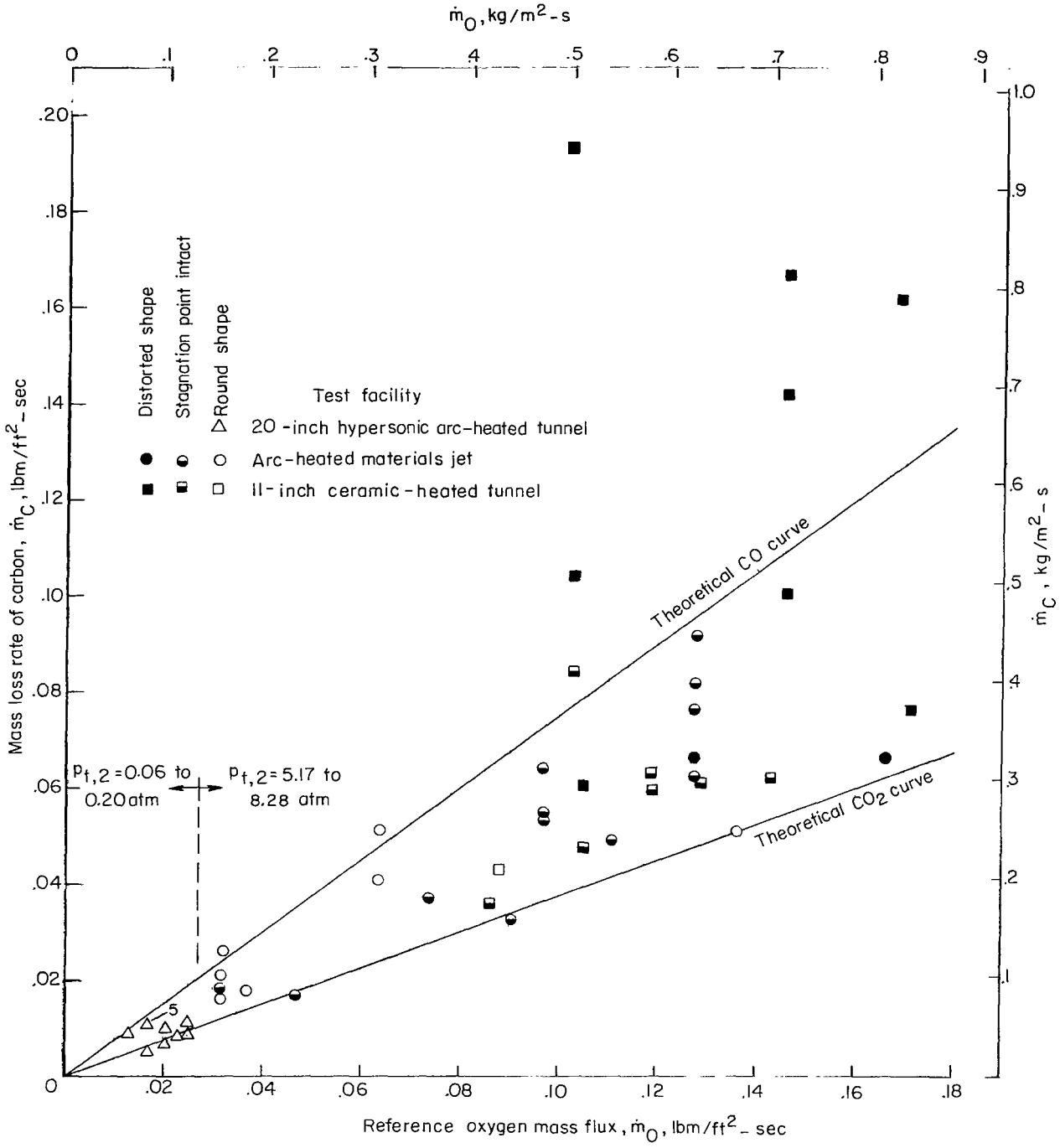

Figure 11.- Comparison of oxidation rates of AHDG graphite with theoretical curves.

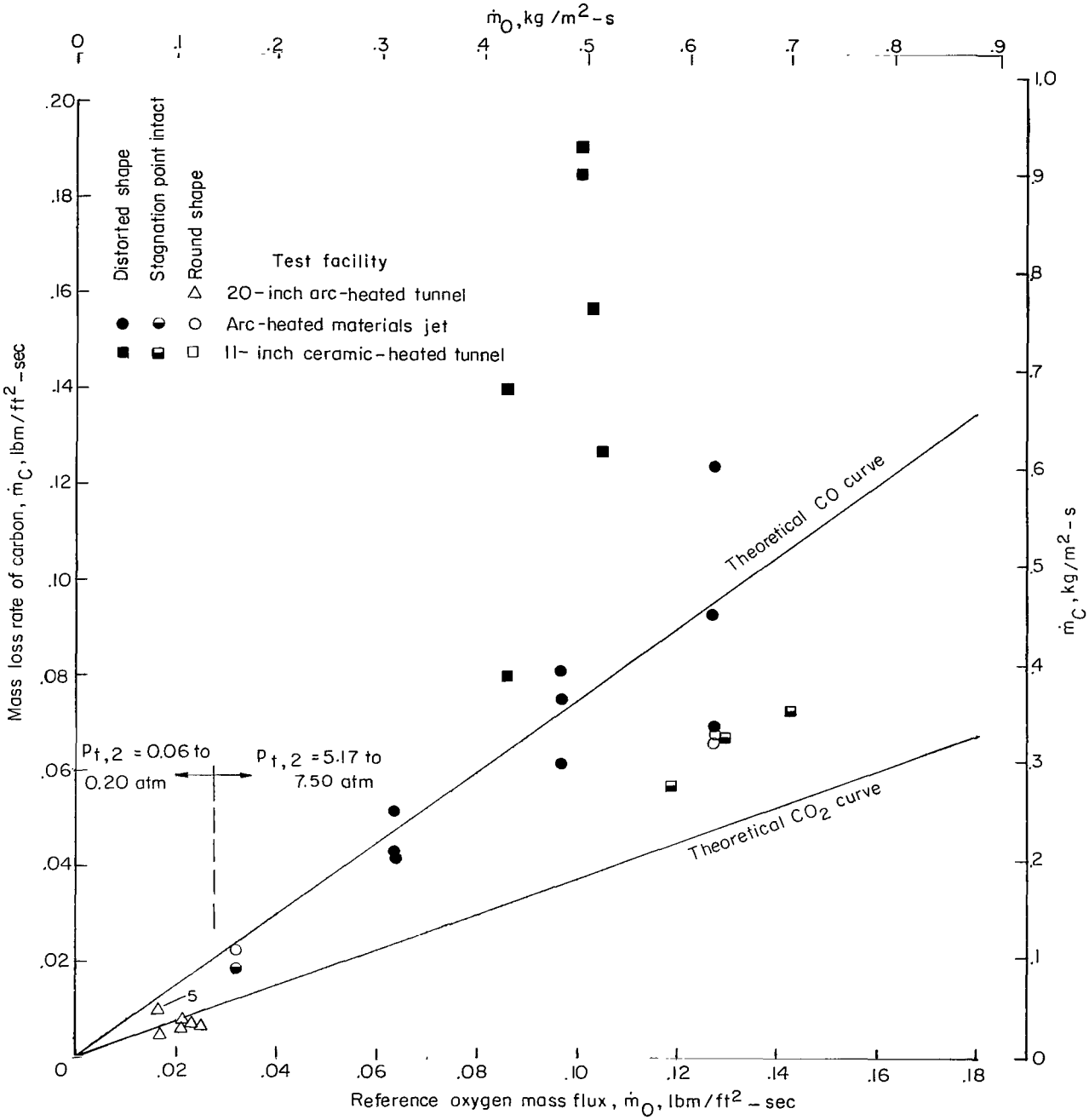

Figure 12.- Comparison of oxidation rates of AGSX graphite with theoretical curves.

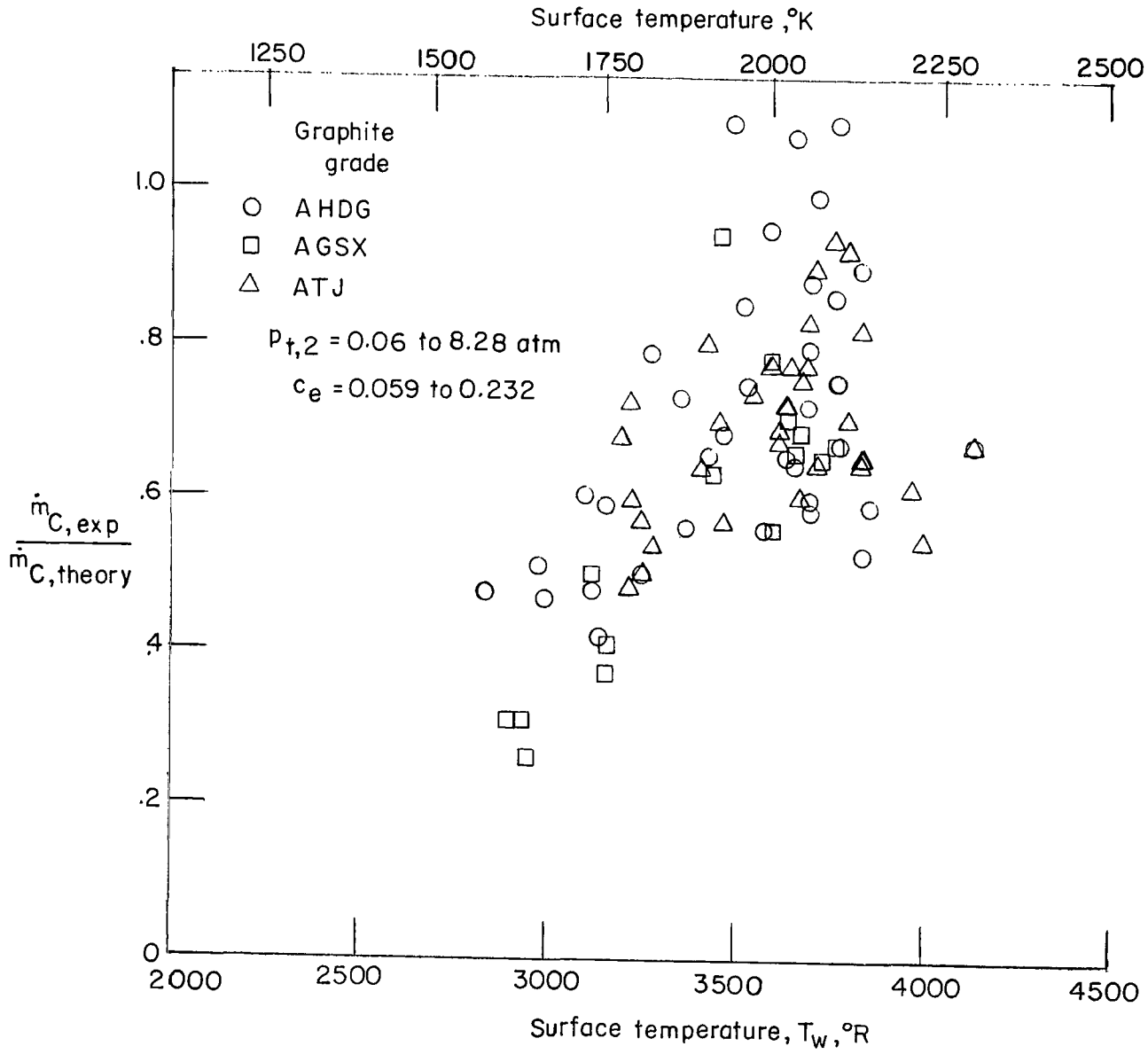

Figure 13.- Normalized graphite oxidation rate as a function of surface temperature.

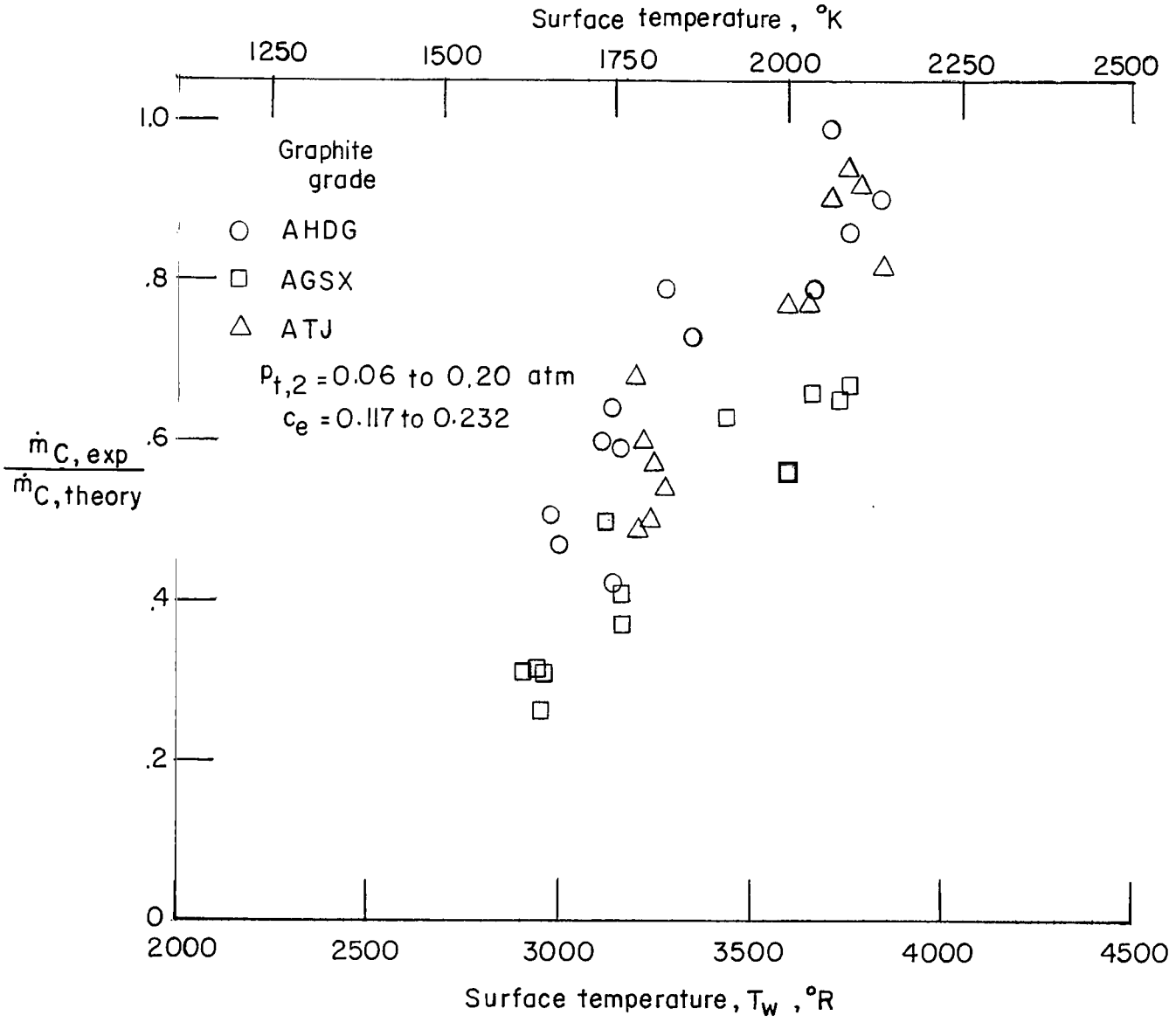

Figure 14.- Normalized graphite oxidation rates as a function of surface temperature and graphite grade at low stagnation pressures.

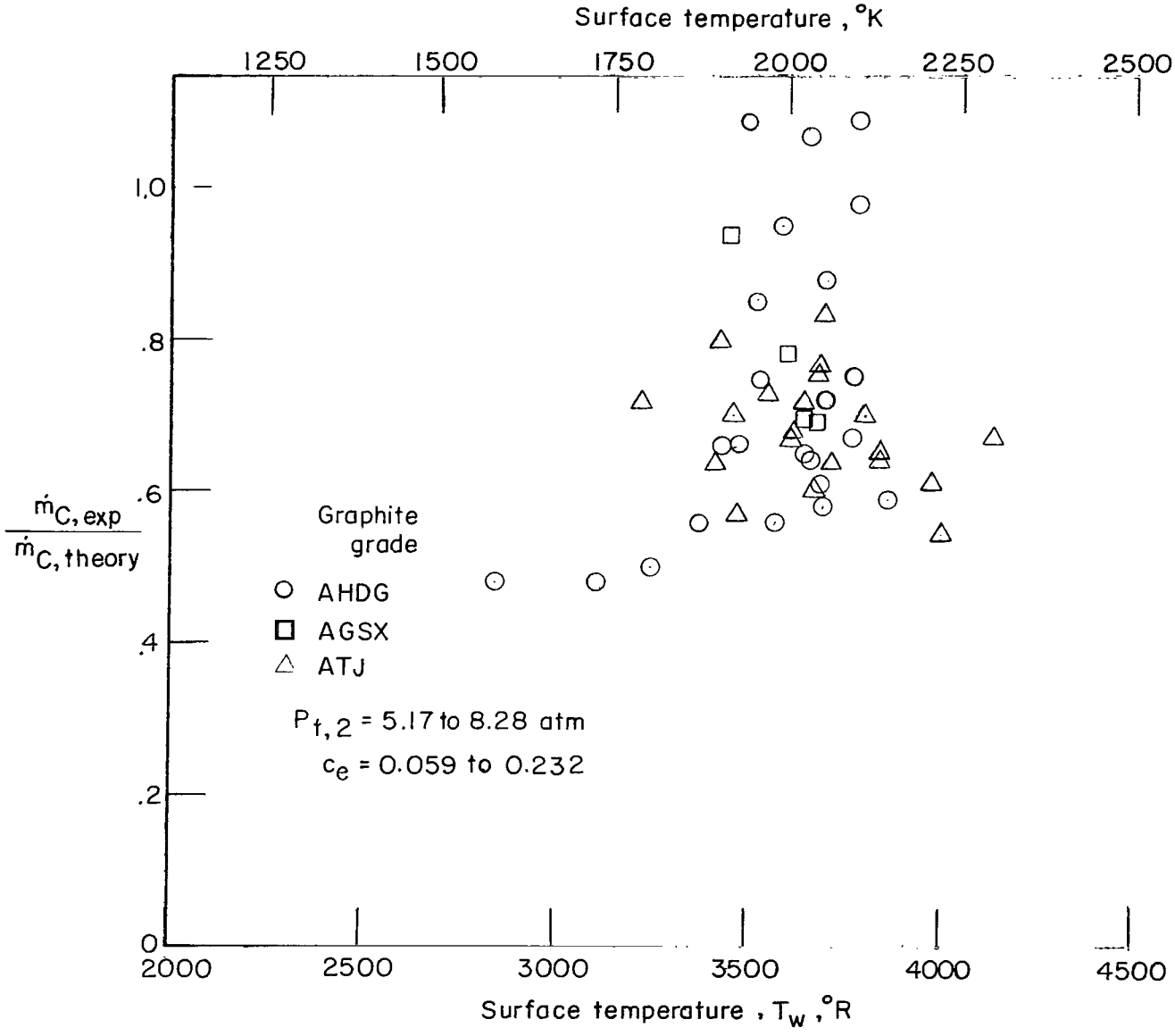

Figure 15.- Normalized graphite oxidation rate as a function of surface temperature at high stagnation pressures.

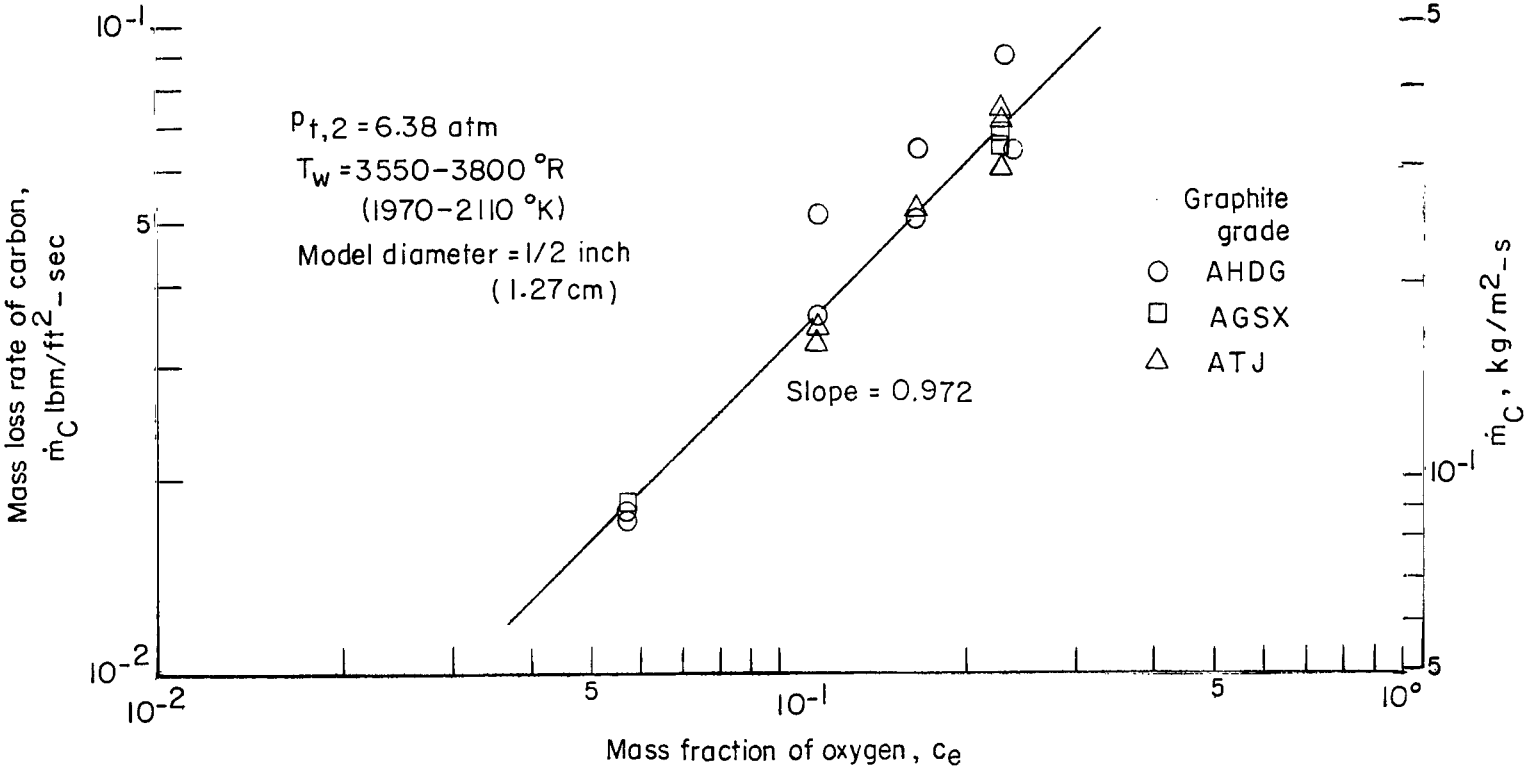

Figure 16.- Graphite oxidation rate as a function of mass fraction of oxygen.

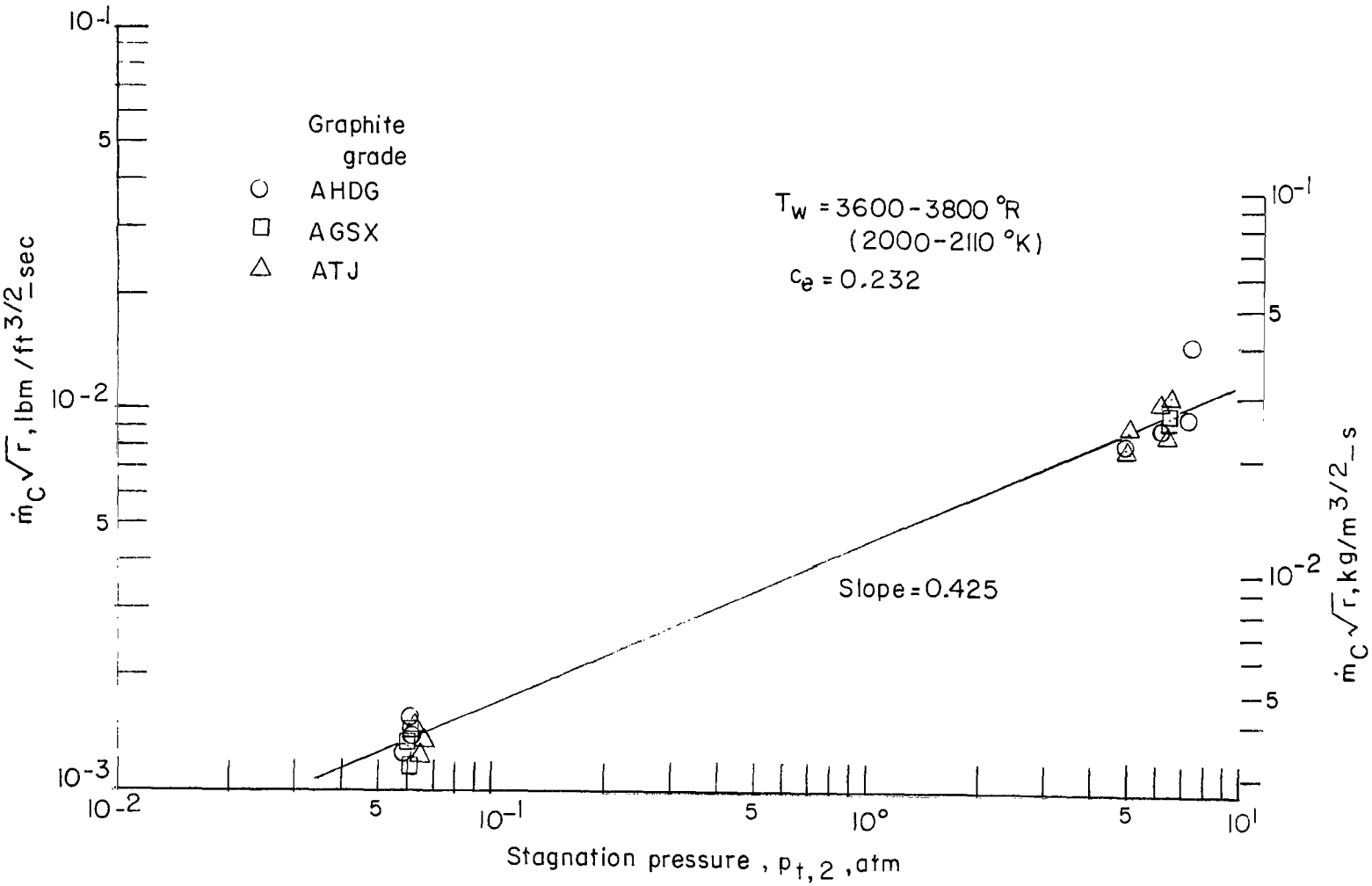

Figure 17.- Graphite oxidation rate × (model radius)$^{1/2}$ as a function of stagnation pressure.

"The aeronautical and space activities of the United States shall be conducted so as to contribute . . . to the expansion of human knowledge of phenomena in the atmosphere and space. The Administration shall provide for the widest practicable and appropriate dissemination of information concerning its activities and the results thereof."

—NATIONAL AERONAUTICS AND SPACE ACT OF 1958

NASA SCIENTIFIC AND TECHNICAL PUBLICATIONS

TECHNICAL REPORTS: Scientific and technical information considered important, complete, and a lasting contribution to existing knowledge.

TECHNICAL NOTES: Information less broad in scope but nevertheless of importance as a contribution to existing knowledge.

TECHNICAL MEMORANDUMS: Information receiving limited distribution because of preliminary data, security classification, or other reasons.

CONTRACTOR REPORTS: Technical information generated in connection with a NASA contract or grant and released under NASA auspices.

TECHNICAL TRANSLATIONS: Information published in a foreign language considered to merit NASA distribution in English.

TECHNICAL REPRINTS: Information derived from NASA activities and initially published in the form of journal articles.

SPECIAL PUBLICATIONS: Information derived from or of value to NASA activities but not necessarily reporting the results of individual NASA-programmed scientific efforts. Publications include conference proceedings, monographs, data compilations, handbooks, sourcebooks, and special bibliographies.

Details on the availability of these publications may be obtained from:

SCIENTIFIC AND TECHNICAL INFORMATION DIVISION

NATIONAL AERONAUTICS AND SPACE ADMINISTRATION

Washington, D.C. 20546